# A numerical study of the topology of hyperbolic manifolds supporting Arnold diffusion in a priori unstable systems.

Massimiliano Guzzo, Elena Lega, Claude Froeschle

**Communications in Mathematical Physics manuscript No.**
(will be inserted by the editor)

# A numerical study of the topology of hyperbolic manifolds supporting Arnold diffusion in a priori unstable systems.

**Massimiliano Guzzo[2],Elena Lega[1], Claude Froeschlé[1]**

[1] Observatoire de Nice, Bv. de l'Observatoire, B.P. 4229,
06304 Nice cedex 4, France.

[2] Università degli Studi di Padova,
Dipartimento di Matematica Pura ed Applicata
via Trieste 63, 35121 Padova, Italy.

**Abstract:** In this paper we study the Arnold diffusion along a normally hyperbolic invariant manifold in a model of a priori unstable system. Using numerical methods we detect global and local properties of the stable and unstable manifolds of the invariant manifold, and we compare them with the diffusion properties. Specifically, we introduce a new definition of Arnold diffusion which is adapted to the numerical investigation of the problem, and we show that the numerically computed stable and unstable manifolds indeed support this kind of Arnold diffusion. We also show that the global topology of the stable and unstable manifolds has a transition when the Melnikov approximation loses its accuracy. The transition is correlated to a change of the law of dependence of the diffusion coefficient on the perturbing parameter. This suggests that the Melnikov approximation is not only a technical tool which allows one to compute accurate approximations of the manifolds at small values of the perturbing parameters, but is related to a dynamical regime.

## 1. Introduction

Diffusion in conservative dynamical systems has been intensively studied in the last decades. Apart from specific examples, the understanding of the general mechanisms which can produce drift and diffusion in the phase space of such systems is an open problem. In this paper we focus our attention on an important class of conservative systems, which we call *a priori unstable* ones following the terminology introduced in [6]. Since the pioneering work of Arnold [1] many efforts have been done to relate diffusion in phase space to the topology of the so called stable and unstable manifolds of the normally hyperbolic invariant manifolds of the system. To fix ideas, we define here the terminology used through this paper.

i) *We study dynamical systems defined by a family of smooth symplectic maps:* $(I', \varphi') = \phi_\epsilon(I, \varphi)$*, with the action–angle variables* $(I, \varphi)$ *defined on the domain* $B \times \mathbb{T}^n$*, with* $B \subseteq \mathbb{R}^n$ *open bounded, and the symplectic structure is* $dI \wedge d\varphi$*. The family* $\phi_\epsilon$ *depends smoothly on the parameter* $\epsilon$*. Some actions* $I_j, \ldots, I_n$*, with* $j > 1$*, are constants of motion of the unperturbed map* $\phi_0$*. Moreover,* $\phi_0$ *has a normally hyperbolic symplectic invariant sub-manifold* $\Lambda_0$ *(the definition of normal hyperbolicity is recalled in section 2). The restriction of* $\phi_0$ *to* $\Lambda_0$ *is an integrable anisochronous map with first integrals* $I_j, \ldots, I_n$. We call such maps a priori unstable. We recall that the restriction of a symplectic map to a symplectic sub-manifold is symplectic with respect to the restricted symplectic form, and the integrability of $\phi_{0|\Lambda_0}$ is intended as the complete integrability of a symplectic map.

ii) *We consider suitably small* $|\epsilon|$ *such that the map* $\phi_\epsilon$ *has a normally hyperbolic symplectic invariant sub-manifold* $\Lambda_\epsilon$ *which is canonically smoothly conjugate to* $\Lambda_0$*. We also require that the KAM theorem for maps applies to the restriction of* $\phi_\epsilon$ *to* $\Lambda_\epsilon$. Here, the reference to KAM theorem is appropriate because, as remarked above, due to the fact that $\Lambda_\epsilon$ is a symplectic sub-manifold, the restriction of the map $\phi_\epsilon$ to $\Lambda_\epsilon$ is symplectic, the map $\phi_{0|\Lambda_0}$ is integrable anisochronous, and $\epsilon$ is therefore the small parameter of KAM theorem.

iii) *For some* $c_0 > 0$*, and any small* $\epsilon$*, we require that any orbit* $(I(t), \varphi(t)) = \phi_\epsilon^t(I(0), \varphi(0))$*, with* $(I(0), \varphi(0)) \in \Lambda_\epsilon$*, satisfies:*

$$\|I(t) - I(0)\| < c_0$$

*for any* $t \in \mathbb{Z}$*.*

We remark that, because of condition (iii), the motions of the map $\phi_\epsilon$ with initial conditions on $\Lambda_\epsilon$ are uniformly bounded in the actions. Therefore, Arnold diffusion concerns the dynamics in neighborhoods of $\Lambda_\epsilon$.

iv) *We say that the problem of Arnold diffusion for* $\phi_\epsilon$ *consists in proving that, for any suitably small* $\epsilon \neq 0$ *and for any neighbourhood* $V$ *of* $\Lambda_\epsilon$ *there exist motions such that for some* $t \in \mathbb{Z}$ *it is:* $(I(0), \varphi(0)), (I(t), \varphi(t)) \in V$*, and*

$$\|I(t) - I(0)\| > 2c_0 \quad . \tag{1}$$

The above definition (iv) of Arnold diffusion is not well suited for the numerical study of the problem, because numerical integrations cannot span any value of the perturbing parameter and any small neighbourhood of $\Lambda$.

Therefore, we give below a definition which is more adapted to the numerical investigation, and it still contains most of the whole complexity of Arnold diffusion.

v) *We say that the problem of the numerical detection of Arnold diffusion for* $\phi_\epsilon$ *in the subset* $\tilde{\Lambda} \subseteq \Lambda_\epsilon$ *consists in the numerical detection of:*

- *two points* $x' = (I', \varphi'), x'' = (I'', \varphi'') \in \tilde{\Lambda}$ *such that the closures* $\mathcal{C}(x'), \mathcal{C}(x'')$ *of their orbits have empty intersection;*
- *two vectors* $\Delta x' = (\Delta I', \Delta\varphi'), \Delta x'' = (\Delta I'', \Delta\varphi'') \in \mathbb{R}^{2n}$*;*
- *a positive* $t \in \mathbb{N}$ *and an index* $k \in \{j, ..., n\}$*;*

*such that:*

- $x' + \Delta x' \in W_u(x')$, *where* $W_u(x')$ *denotes the unstable manifold of* $x'$*;*
- $\phi_\epsilon^t(x' + \Delta x') + \Delta x'' \in W_s(x'')$, *where* $W_s(x'')$ *denotes the stable manifold of* $x''$*;*
- *for any* $(\tilde{I}', \tilde{\varphi}') \in \mathcal{C}(x')$, $(\tilde{I}'', \tilde{\varphi}'') \in \mathcal{C}(x'')$ *it is:*

$$\left| \tilde{I}'_k - \tilde{I}''_k \right| > c_k + |\Delta I'_k| + |\Delta I''_k| \tag{2}$$

*where* $c_k$ *is such that any orbit* $(I(h), \varphi(h)) = \phi_\epsilon^h(I(0), \varphi(0))$, *with* $(I(0), \varphi(0)) \in \tilde{\Lambda}$, *satisfies:*

$$|I_k(h) - I_k(0)| < c_k \quad \forall \quad h \in \mathbb{Z} \quad ;$$

*for some values of the perturbing parameter satisfying (ii) and (iii).*

We remark that condition (v) is never fulfilled by the unperturbed map $\phi^0$, because in such a case the actions $I_j, \ldots, I_k$ are constants of motion.

The above definition is clearly inspired by the proofs of existence of Arnold diffusion which show that the stable and unstable manifolds of different invariant tori of $\Lambda_\epsilon$ intersect transversely (for a precise statement we refer to [6]). The sequence of such invariant tori is called transition chain and the shadowing argument which is used to prove diffusion through the transition chain is called transition chain mechanism. Therefore, on the one hand condition (v) is weaker than condition (iv) because it refers to finite values of $\epsilon$ and to specific neighbourhoods of $\Lambda$ (determined by $\Delta x'$, $\Delta x''$), on the other hand condition (v) provides also a numerical verification of the topological mechanism which is behind the diffusion of the actions. In section 6 we provide an example of numerical detection of Arnold diffusion for which, equation (2) is verified within the numerical errors, i.e. with the notations of (v), we numerically find:

$$\left| \tilde{I}'_k - \tilde{I}''_k \right| > c_k + |\Delta I'_k| + |\Delta I''_k| + \rho \quad , \tag{3}$$

where $\rho > 0$ is an estimation of the numerical errors.

The existence of the transition chain mechanism in a specific quasi–integrable system has been proved for the first time by Arnold, and up to now it has not been yet generalized to generic quasi–integrable Hamiltonian systems. A non generic feature of Arnold's example is that the invariant manifold, along which Arnold proves the existence of diffusion, is fibered by invariant tori for all values of the perturbing parameters, i.e. the restriction of the dynamical system to the invariant manifold is integrable. Generalizations of Arnold's example consider normally hyperbolic invariant manifolds $\Lambda_\epsilon$ such that the restriction of the dynamics to $\Lambda_\epsilon$ is not integrable. As a consequence, the distribution of the invariant tori on $\Lambda_\epsilon$ has gaps which correspond to the resonances of the restricted dynamical system. In [6] it is proved the existence of transition chains in regions of the invariant manifold which do not contain a selected number of main resonances. In a more recent paper [8] transition chains crossing the main resonances are constructed by including also stable and unstable manifolds of invariant sets of $\Lambda_\epsilon$ which are topologically different from invariant tori. The existence of diffusing motions has been proved also in [2], [3], [4] using different models and techniques, including variational methods based on Mather theory, and in [30], [31] using the so called separatrix map.

One of the most important techniques to prove the existence of transitions chains (used in [6], [8], [30], [31]) is the so–called Melnikov theory, which provides first order approximations of the stable and unstable manifolds.

Arnold's paper motivated also a great debate about the possibility of numerical detection of Arnold diffusion. While numerical detections of chaotic motions appeared in the sixties in [17], problems related to the numerical detection of Arnold diffusion were already discussed in [7]. In the following decades, many authors studied numerically the diffusion through resonances, referring to it as Arnold diffusion. In some papers related to applications we find explicit reference to possible interpretations of numerical diffusion as Arnold diffusion (such as, for example [22]); other papers, such as [33], [25], [21], studied the numerical diffusion of orbits in coupled standard maps by changing the perturbation parameters and the number of coupled maps (for a review see also [24] and references therein). Detailed computations of the stable and unstable manifolds of hyperbolic tori related to an Arnold diffusion problem can be found in [29]. In [23], [15], [13] we studied the diffusion of orbits in quasi–integrable systems for values of the perturbing parameters for which there is numerical evidence of applicability of the KAM and Nekhoroshev theorems. Despite of the slowness of the diffusion in quasi–integrable systems, we were able to measure a statistical regularity in the diffusion properties of well chosen sets of initial conditions, in the following sense:

vi) *we say that a set of $N$ initial conditions diffuse in the phase space with regular statistics if the average evolution of the squared distance of the actions from their initial value grows linearly with time; i.e. there exists a constant $D > 0$, which we call diffusion coefficient, such that:*

$$\frac{\sum_{j=1}^{N} |I^{(j)}(t) - I^{(j)}(0)|^2}{N} \sim D\ t \quad . \tag{4}$$

*The numerical detection of sets of orbits diffusing with regular statistics in the time interval $[0, T]$ means that the linear law (4) is verified by means of a $\chi^-$ square fit over the interval $[0, T]$ with correlation coefficient larger than 0.9.*

The detailed statistical characterization of Arnold diffusion is described in section 7.

Relating the Arnold diffusion of orbits with regular statistics to the topology of the stable and unstable manifolds of $\Lambda_\epsilon$ remains a delicate matter. In this paper we investigate this problem by numerically computing the topological structures which support the Arnold diffusion defined in (v) in a specific example of systems (i) satisfying (ii) and (iii) and by comparing them with the diffusion coefficient defined in (vi) (and in section 7).

For the first time we provide global representations of the stable and unstable manifolds of the normally hyperbolic invariant manifold of the system, and not only of some specific hyperbolic tori. We use different numerical methods to represent the stable and unstable manifolds of the invariant manifold $\Lambda_\epsilon$ embedded in the higher dimensional phase space. More precisely we use a traditional method based on sets propagation and we introduce a new one based on the so called Fast Lyapunov Indicator, defined in [10].

We measure a spread of the asymptotic stable (unstable) manifolds in the phase–space which is significant to explain Arnold diffusion in the sense stated by (v).

We show that the topology of the stable and unstable manifolds of $\Lambda_\epsilon$ has a transition when the perturbing parameter is so large that the Melnikov approximation is no more valid. Moreover, when the Melnikov approximation is valid, we measure diffusion coefficients which can be fitted by a $D \sim \epsilon^2$ law. Instead, when the Melnikov approximation is not valid we find that the $D \sim \epsilon^2$ fit breaks down. This suggests us that for these systems the Melnikov approximation is not only a technical tool which allows one to compute accurate approximations of the manifolds at small values of the perturbing parameters, but is related to the topology of the stable and unstable manifolds of $\Lambda_\epsilon$ and to a specific dependence of $D \sim \epsilon^2$ on $\epsilon$. All these properties define the Melnikov regime of the system.

We remark that the transition related to the Melnikov regime occurs for values of the perturbing parameter within the range of validity of the KAM theorem for the restriction of the map to the invariant manifold.

The paper is organized as follows: in section 2 we recall some definitions about the normally hyperbolic invariant manifolds and we define our model example; in section 3 we recall the dynamical properties of a priori–unstable systems which are useful in this paper; in section 4 we describe the numerical methods for detecting the structure of the stable (unstable) manifolds; in section 5 we report the results on the computation of the stable (unstable) manifolds and the comparison with the Melnikov approximation; in section 6 we relate the geometry of the manifolds to diffusion; in section 7 we describe the statistical analysis of Arnold diffusion.

## 2. Hyperbolic invariant manifolds in a model problem

The notion of normally hyperbolic invariant manifolds is extensively studied in [19], and can be stated as follows (see, for example, [19], [18]):

**Definition.** *Let $M$ be a $\mathcal{C}^q$ ($q \geq 1$) compact connected manifold; let $U \subseteq M$ open and let $\phi : U \to M$ be a $\mathcal{C}^q$ embedding; let $\Lambda$ be a sub-manifold of $M$ which is invariant by $\phi$. The map $\phi$ is said to be normally hyperbolic to $\Lambda$ ($\Lambda$ is also said to be normally hyperbolic invariant manifold) if there exists a Riemannian structure on $M$ such that for any point $x \in \Lambda$ the tangent space $T_xM$ has the following splitting:*

$$T_xM = E^s(x) \oplus T_x\Lambda \oplus E^u(x)$$

*which is continuous, invariant, i.e. the linear spaces $E^s(x), E^u(x)$ are invariant by $\phi$:*

$$D\phi E^s(x) \subseteq E^s(\phi(x)) \quad , \quad D\phi E^u(x) \subseteq E^u(\phi(x)) \quad ,$$

*and there exist constants $\lambda_1, \lambda_2, \lambda_3, \mu_1, \mu_2, \mu_3$ satisfying:*

$$0 < \lambda_1 \leq \mu_1 < \lambda_2 \leq \mu_2 < \lambda_3 \leq \mu_3 \quad , \quad \mu_1 < 1 < \lambda_3 \quad , \tag{5}$$

*such that:*

$$\lambda_1 \leq \inf_{\xi \in E^s(x)\setminus 0} \frac{\|D\phi(x)\xi\|}{\|\xi\|} \leq \sup_{\xi \in E^s(x)\setminus 0} \frac{\|D\phi(x)\xi\|}{\|\xi\|} \leq \mu_1$$
$$\lambda_2 \leq \inf_{\xi \in T_x\Lambda\setminus 0} \frac{\|D\phi(x)\xi\|}{\|\xi\|} \leq \sup_{\xi \in T_x\Lambda\setminus 0} \frac{\|D\phi(x)\xi\|}{\|\xi\|} \leq \mu_2$$

$$\lambda_3 \leq \inf_{\xi \in E^u(x)\setminus 0} \frac{\|D\phi(x)\xi\|}{\|\xi\|} \leq \sup_{\xi \in E^u(x)\setminus 0} \frac{\|D\phi(x)\xi\|}{\|\xi\|} \leq \mu_3 \quad . \tag{6}$$

An important property of normally hyperbolic invariant manifolds is represented by the existence of the so called local stable (unstable) manifold. Precisely, for any $x \in \Lambda$ there exist the smooth manifolds $W_s^{loc}(x), W_u^{loc}(x)$ (see [19]) such that: $x \in W_s^{loc}(x), W_u^{loc}(x)$, $T_x W_s^{loc}(x) = E^s(x)$, $T_x W_u^{loc}(x) = E^u(x)$ and for any $n \geq 0$ it is:

$$y \in W_s^{loc}(x) \quad \Rightarrow \quad d(\phi^n(x), \phi^n(y)) \leq C(\mu_1 + c)^n d(x, y)$$

$$y \in W_u^{loc}(x) \quad \Rightarrow \quad d(\phi^{-n}(x), \phi^{-n}(y)) \leq C(\lambda_3 - c)^{-n} d(x, y)$$

with $C, c > 0$ suitable constants ($c$ suitably small) and $d(\cdot, \cdot)$ denotes a distance on $M$. The manifolds $W_s(x), W_s(x)$ are then obtained by iterating the local manifolds $W_s^{loc}(x), W_u^{loc}(x)$ with $\phi^{-1}$ and $\phi$ respectively.

The local stable and unstable manifolds of $\Lambda$ are defined by:

$$W_s^{loc} = \cup_{x \in \Lambda} W_s^{loc}(x) \quad , \quad W_u^{loc} = \cup_{x \in \Lambda} W_u^{loc}(x) \quad , \tag{7}$$

while the stable and unstable manifolds of $\Lambda$ are:

$$W_s = \cup_{x \in \Lambda} W_s(x) \quad , \quad W_u = \cup_{x \in \Lambda} W_u(x) \quad , \tag{8}$$

**Examples.** The explicit examples given in this paper refer to the discrete system defined by the map:

$$\begin{array}{c} \phi_\epsilon : \mathbb{R}^2 \times \mathbb{T}^2 \longrightarrow \mathbb{R}^2 \times \mathbb{T}^2 \\ (\varphi_1, \varphi_2, I_1, I_2) \longmapsto (\varphi_1', \varphi_2', I_1', I_2') \end{array} \tag{9}$$

such that:

$$\begin{aligned} \varphi_1' &= \varphi_1 + I_1 \\ \varphi_2' &= \varphi_2 + I_2 \\ I_1' &= I_1 - a \sin \varphi_1' + \epsilon \frac{\sin \varphi_1'}{(\cos \varphi_1' + \cos \varphi_2' + c)^2} \\ I_2' &= I_2 + \epsilon \frac{\sin \varphi_2'}{(\cos \varphi_1' + \cos \varphi_2' + c)^2} \quad , \end{aligned} \tag{10}$$

where $a, \epsilon$ and $c > 2$ are parameters. The symplectic structure on $\mathbb{R}^2 \times \mathbb{T}^2$ is $d\varphi_1 \wedge dI_1 + d\varphi_2 \wedge dI_2$. The map $\phi_\epsilon$ has the following invariant manifold:

$$\Lambda = \{(I_1, \varphi_1, I_2, \varphi_2) : \quad \text{such that} \quad (I_1, \varphi_1) = (0, \pi)\} \tag{11}$$

for any value of the parameters. In particular we will consider the following cases:

*i)* For $a > 0$ and $\epsilon = 0$ the manifold $\Lambda$ is normally hyperbolic. For example, one can easily define constants $\lambda_1, \ldots, \mu_3$ satisfying (6) with reference to the following flat norm of tangent vectors $\|(\xi_{\varphi_1}, \xi_{\varphi_2}, \xi_{I_1}, \xi_{I_2})\|^2 = |\xi_{\varphi_1}|^2 + \gamma |\xi_{\varphi_2}|^2 + |\xi_{I_1}|^2 + |\xi_{I_2}|^2$, with $\gamma \in (0, 1]$ suitably small. An alternative way to display the normal hyperbolicity of the map is to fix a Riemannian structure (for example

with $\gamma = 1$) and then finding and integer $N$ such that the map $\phi_0^N$ is normally hyperbolic.

The stable and unstable manifolds of $\Lambda$ are the product of the stable and unstable manifolds of the hyperbolic fixed point of the standard map:

$$\varphi_1' = \varphi_1 + I_1 \quad , \quad I_1' = I_1 - a \sin \varphi_1'$$

with the torus $\mathbb{R} \times \mathbb{T}$, domain of $(I_2, \varphi_2)$. Because normal hyperbolicity persists for small perturbations, $\Lambda$ is normally hyperbolic also for the map $\phi_\epsilon$ with suitably small $\epsilon$. In this case the stable and unstable manifolds are not a product as in the previous case, and to describe their topology we will use Melnikov–like approximations and numerical techniques. We remark that the family $\phi_\epsilon$ defines an a priori unstable system according to definition (i) given in the introduction. For the sake of simplicity, in the rest of the paper we use the notation $\phi$ instead of $\phi_\epsilon$.

*ii)* For $a = 0$, $\epsilon = 0$ the map is integrable and $\Lambda$ is not hyperbolic. For $a = 0$ and $\epsilon \neq 0$ the map is quasi–integrable, the manifold $\Lambda$ is still invariant (as well as the manifold $(I_2, \varphi_2) = (0, \pi)$), but one does not immediately recognize if it is hyperbolic. The Arnold diffusion in this quasi–integrable map has been studied in [23], [15], [13].

## 3. Survey on the dynamics near hyperbolic invariant manifolds in the model problem

The dynamics of $\phi$ defined in (10) restricted to $\Lambda$ has no diffusion if $\epsilon$ is suitably small. In fact, this dynamics is represented by the 2–dimensional map:

$$\varphi_2' = \varphi_2 + I_2 \quad , \quad I_2' = I_2 + \epsilon \frac{\sin \varphi_2'}{(\cos \varphi_2' + c - 1)^2} \quad , \tag{12}$$

whose invariant KAM curves exclude any possibility of diffusion for $I_2$ if $\epsilon$ is suitably small. Let us fix an interval $D$ of the action $I_2$ and denote by $\epsilon_c$ the value such that the KAM theorem is valid in a open domain containing $D \times \mathbb{T}$ for any $0 = \epsilon \leq \epsilon_c$. As usual in KAM theory, the analytic estimate of $\epsilon_c$ can be inefficient, so that we refer to its numerical estimate obtained directly from the phase portraits of the restricted map. From the analysis of numerically computed phase portraits of (12), with $c = 2.1$, in the interval $I_2 \in D = [0.26, 0.38]$ we obtain that for $0 \leq \epsilon < 0.002$ the map has still many invariant tori which constitute a topological barrier to the diffusion of the action $I_2$. Instead, for $\epsilon = 0.0026$ the invariant tori seem to have disappeared, leaving the possibility of chaotic diffusion in the direction of the action $I_2$. Therefore, there is a numerical indication that $\epsilon_c \in (0.002, 0.0026)$. We recall that if the invariant tori are a topological barrier which completely stops diffusion, as soon as $\epsilon$ is bigger than $\epsilon_c$ there is the possibility of diffusion, but it can be very slow because of possible stickiness phenomena (see, for example, [9]) due to the presence of cantori and islands of regular motion [26]. These barriers to diffusion loose their effectiveness at higher values of $\epsilon$.

We remark that, because the perturbation in (12) has a full Fourier expansion, all the gaps in the distribution of invariant KAM tori scale with the perturbation parameter by order $\sqrt{\epsilon}$. This situation represents the worst possible distribution

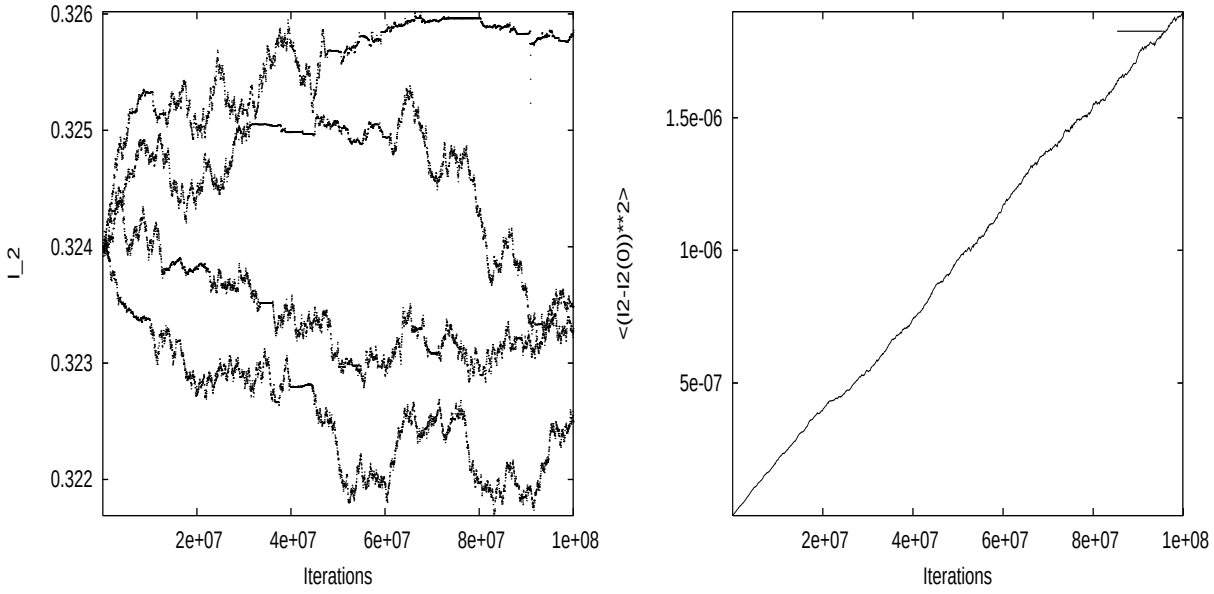


**Fig. 1. On the left:** Evolution of $I_2$ as a function of time for four orbits of initial conditions $I_1 = -10^{-5}, -10^{-6}, 10^{-6}, 10^{-5}$, $I_2 = 0.324$, $\varphi_1 = \pi$, $\varphi_2 = 0$ and $\varepsilon = 10^{-7}$. **On the right:** Evolution with time of the mean square distance of a set of $N = 1000$ orbits form their initial conditions. The initial conditions are: $I_1 \in [-10^{-5}, 10^{-5}]$, $I_2 = 0.324$, $\varphi_1 = \pi$, $\varphi_2 = 0$ and $\varepsilon = 10^{-7}$.

of gaps which is compatible with the KAM theorem, and therefore (10) represents a robust test for Arnold diffusion investigations.

In this paper we are interested in the range $0 < \epsilon < \epsilon_c$, for which there is not diffusion on $\Lambda$ and we study the diffusion properties of a neighborhood of $\Lambda$. This can be done numerically with the techniques which we used in [11], [23], [15], [13], [16] to study Arnold diffusion in quasi–integrable systems. Specifically:

i) we find that individual orbits in a neighborhood of the invariant manifold indeed spread in the $I_2$ direction, as it is shown in figure 1 (left panel). The evolution of the action $I_2$ is characterized by many oscillations and temporary captures, while the evolution of the square distance of the action from its initial value averaged over many initial conditions shows an approximate linear growth (see figure 1, right panel), as in the diffusion processes defined in (vi).

ii) we measured the diffusion coefficient for $a = 0.4$, $c = 2.1$ for different values of $\epsilon$ for three sets of $N = 100$ initial conditions with $I_2 = 0.324$, $I_2 = 1.8$ and $I_2 = 2$ respectively (the other initial conditions are $I_1 \in [-10^{-5}, 10^{-5}]$, $\varphi_1 = \pi$, $\varphi_2 = 0$). The average evolution of the mean squared distance of the action $I_2$ from its initial value grows almost linearly with time for most values of $\epsilon$, the slope giving the diffusion coefficient according to (vi), which we estimate using the method (m2) described in section 7. Here, we describe the results of the computation, which are reported in figure 2. For the three sets of initial conditions the diffusion coefficient is well fitted by a power law $D(\epsilon) \simeq \epsilon^2$ for $\epsilon \leq 6\ 10^{-6}$. For $6\,10^{-6} \leq \epsilon \leq 4\,10^{-4}$ some irregularity can appear depending on

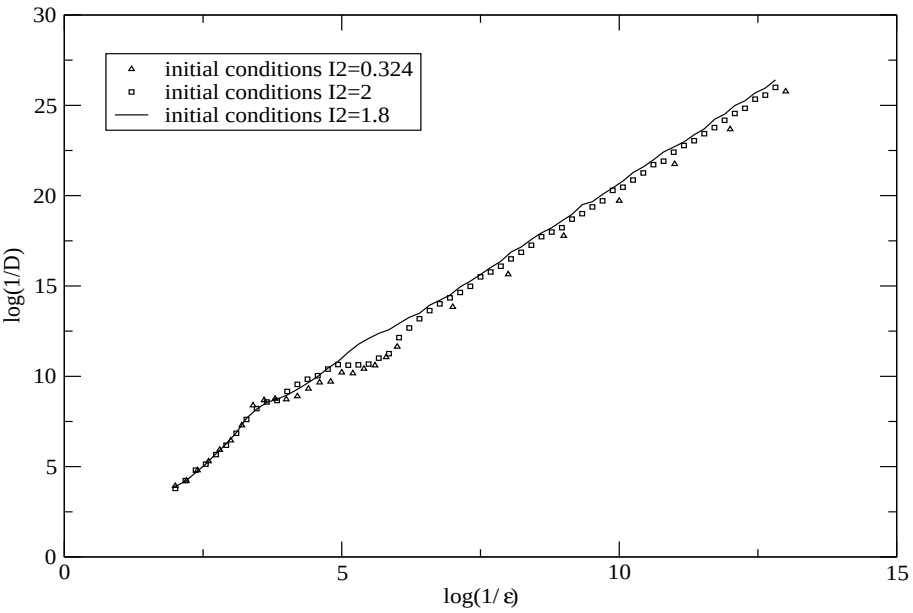


**Fig. 2.** Variation of the diffusion coefficient as a function of $\epsilon$, for $a = 0.4$ and $c = 2.1$. Data are very well fitted to a power law $D(\epsilon) \simeq \epsilon^2$ for $10^{-13} \leq \epsilon \leq 6\,10^{-6}$. For $6\,10^{-6} \leq \epsilon \leq 4\,10^{-4}$ some irregularity can appear depending on the choice of initial conditions, although data are not far from the $D(\epsilon) \simeq \epsilon^2$ law. The correlation coefficient turns out to be lower than 97% in the interval $5\,10^{-6} < \epsilon < 5\,10^{-4}$ with a minimum value of 84% for $\epsilon = 1.2\,10^{-5}$ for the set of data with initial conditions centered on $I_2 = 2$. The diffusion coefficients are estimated following method (m2) described in section 7.

the specific set of initial conditions, although data are not far from the $D(\epsilon) \simeq \epsilon^2$ law. For $\epsilon > 4\ 10^{-4}$ the power law changes to $D(\epsilon) \simeq \epsilon^{2.8}$. We anticipate (see section 5) that these changes in the law of dependence of $D$ on $\epsilon$ seem to be correlated to changes in the topology of the stable (unstable) manifolds of $\Lambda$.

These experimental facts can be only partially explained by means of existing rigorous results. Precisely, though there does not exist in the literature a rigorous result proving diffusion of orbits for a system like (10), this system is very similar to those studied in [4], [6], [30], [31], [8], for which diffusion of individual orbits is proved. The differences between the map (10) with $a \neq 0$ and the systems studied in those papers are: for $\epsilon = 0$ the system studied in [4], [6], [30], [31], [8] is a simple pendulum coupled with a rotation (a more general case is considered in [6], [30], [31], which includes perturbations of such a system), while for the map (10) the unperturbed case corresponds to a standard map coupled with a rotation. However, in both cases there is an invariant manifold which is hyperbolic also at $\epsilon = 0$; the dynamics on this invariant manifold can be represented by a 2D quasi–integrable map. As a consequence, the mechanism of transition introduced in [8] which takes into account the stable and unstable manifolds of all type of orbits (not only the invariant tori) could be important also in the present case. The techniques used in [8] are essentially based on the Melnikov approximation of

the stable and unstable manifolds of the normally hyperbolic invariant manifold, which, in the continuous case, is well expressed through explicit integrals. The techniques used in [30], [31] are based on the so–called separatrix map method, which is based on the Melnikov approximation as well.

Here, a Melnikov like approximation, which will be introduced in section 5, is instead based on series expansions. We will compare numerically in section 5 the Melnikov approximations of the stable and unstable manifolds with the representation obtained by the numerical methods described in section 4.

## 4. Numerical detection of the stable and unstable manifolds

In this section we describe the methods which we use to detect numerically the global structure of the stable and unstable manifolds of a two dimensional normally hyperbolic invariant manifold of a four dimensional map. We will use two different methods displaying different properties of the global structure of these manifolds. The first one is based on the method of propagation of sets commonly used to detect the stable and unstable manifolds of hyperbolic fixed points of two dimensional maps; the second one is based on the computation of the fast Lyapunov indicator (FLI in the following, see [10]).

It is well known that the numerical localization of the unstable manifold of an hyperbolic fixed point can be obtained by propagating a small neighborhood of initial conditions up to a time $T$ of the order of some Lyapunov times of the fixed point. In such a way, one directly constructs a neighborhood of a finite piece of the unstable manifold (for the stable manifold one repeats the construction for the inverse flow). This method gives very good results for fixed points of two dimensional maps, because the neighborhoods of the fixed points are two dimensional and can be propagated with reasonable CPU times. A more sophisticated method providing high precision computations and good visualizations of a piece of the manifold can be found in [28].

For higher dimensional maps and higher dimensional invariant hyperbolic manifolds the application of this method encounters two difficulties: the propagation of high dimensional sets requires very long CPU times and the interpretation of the results in an high dimensional space is difficult.

The first problem can be overcome if one knows in advance some approximations of the local unstable manifold to restrict the choice of the set of points to propagate. The second problem could be overcome by reproducing two dimensional sections of the stable and unstable manifolds. However, only few points of the numerically integrated discrete orbits pass near the selected section, so that good results still require enormous sets of initial conditions.

Different sophisticated methods can be found in the literature for computing (un)stable manifolds for higher dimensional cases. The reader can find in [20] a detailed review with applications to the visualization of a 2 dimensional manifold. The common point to all these methods is that the manifolds are "grown" from local knowledge, i.e. from linear approximations. Then the manifold is constructed as a sequence of geodesic curves (see [20]). For the specific case of interest here, i.e. for normally hyperbolic invariant manifolds, an algorithm based on graph transform and Newton's method can be found in [5]. A technique specifically adapted to compute stable manifolds of hyperbolic tori is described in [29]. The first method that we use (method (1) below) adapts these

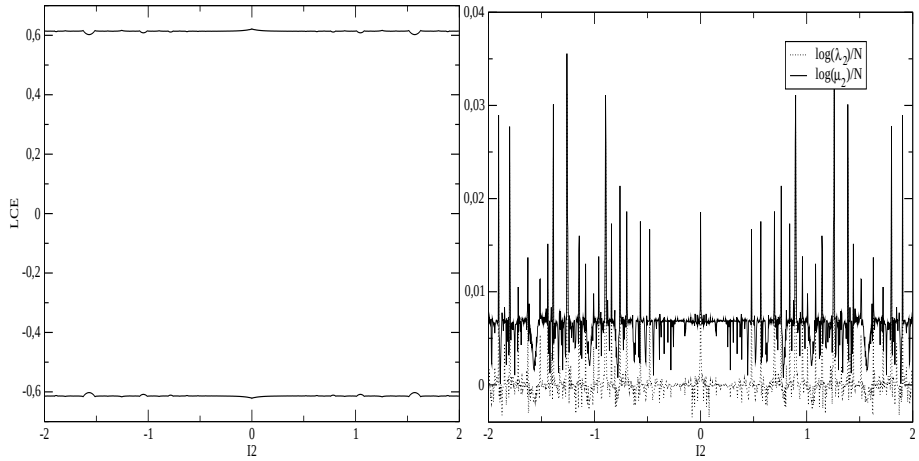


**Fig. 3. On the left:** Lyapunov exponents computed on a grid of 1000 initial conditions with $I_2 \in [-2, 2]$, $I_1 = 0$, $\varphi_1 = \pi$, $\varphi_2 = 0$, on $N = 10^3$ iterations for $\epsilon = 10^{-3}$. The initial tangent vectors are chosen in the space $T_x\Lambda^{ort}$. A positive and a negative value indicate the splitting of $T_x\Lambda^{ort}$ in a stable and an unstable space. **On the right:** Numerical estimates of $\log \lambda_2/N$ and $\log \mu_2/N$, computed on a grid of 1000 initial conditions with $I_2 \in [-2, 2]$, $I_1 = 0$, $\varphi_1 = \pi$, $\varphi_2 = 0$.

known techniques (for example of [28]) to the present case. The second method (method (2) below) is a new application of fast Lyapunov indicators which allows us to compute the intersection of the (un)stable manifolds with a given section of the phase–space.

### 1) Computation and parametrization of $W_s(x)$ using traditional methods of sets propagation.

To discuss the properties of the stable and unstable manifolds we need a precise parametrization of these manifolds.

For all values of the parameters $a, \epsilon$ the dynamics of $\phi_{|\Lambda}$ is defined by the map (12) which can have invariant $KAM$ curves, resonant regular orbits, resonant chaotic orbits. For the moment we consider $x \in \Lambda$ belonging to a KAM curve of $\phi_{|\Lambda}$, but we will apply the method also to the other cases. Below, we explain in detail the steps allowing us to construct numerical parameterizations of the manifolds. These steps are essentially based on standard techniques which allow one to compute stable/unstable manifolds of invariant objects (such as, for example, [28]).

*i) Verification that the manifold $\Lambda$ is normally hyperbolic.* We numerically check that the invariant manifold $\Lambda$ is normally hyperbolic for $\epsilon = 0.001$, which is the largest value of the perturbing parameter for which we compute stable and unstable manifolds. Precisely, we check that a compact invariant region of $\Lambda$, such as the one delimited by two invariant KAM curves containing $(I_2, \varphi_2) = (\pm 2, 0)$, is normally hyperbolic with respect to the map $\phi^N$ for some integer $N$.

For each point $x$ of a grid of initial conditions with $I_2 \in [-2, 2]$, $I_1 = 0$, $\varphi_1 = \pi$, $\varphi_2 = 0$ we first computed the Lyapunov exponents of the map $\phi$ (up

to $N = 10^3$ iterations) for initial tangent vectors in the tangent space $T_x\Lambda^{ort}$ orthogonal to $T_x\Lambda$, i.e. for vectors of the form $\xi = (\xi_{\varphi_1}, 0, \xi_{I_1}, 0)$. We measured a positive Lyapunov exponent bigger than 0.6 for all the points of the grid, and of course a negative Lyapunov exponent smaller than $-0.6$ (figure 3, left panel). This is an indication of the hyperbolic splitting of the space $T_x\Lambda^{ort}$ as a direct sum of a stable space $E^s(x)$ and an unstable space $E^u(x)$. The numerical algorithm for the computation of the Lyapunov characteristic exponents provides also an estimate of $\lambda_1 = \mu_1$ and $\lambda_3 = \mu_3$ related to $\phi^N$. It remains to estimate the constants $\lambda_2, \mu_2$ for the map $\phi^N$ in the point $x$. Because in this case the growth of initial tangent vectors $\xi = (0, \xi_{\varphi_2}, 0, \xi_{I_2}) \in T_x\Lambda$ is not always exponential, we did not compute the Lyapunov characteristic exponents, but we computed numerically the two dimensional matrix representing the restriction of $D\phi^N(x)$ to the space $T_x\Lambda$ and the quantities:

$$\lambda_2 \leq \inf_{\xi \in T_x\Lambda \setminus 0} \frac{\|D\phi^N(x)\xi\|}{\|\xi\|} \leq \sup_{\xi \in T_x\Lambda \setminus 0} \frac{\|D\phi^N(x)\xi\|}{\|\xi\|} \leq \mu_2 \quad .$$

Figure 3 (right panel) shows the numerical computation of $\log \lambda_2/N$ and $\log \mu_2/N$ for $N = 1000$. From the comparison of the four computed quantities $\log \lambda_1$, $\log \lambda_2$, $\log \mu_2$, $\log \lambda_3$ we infer that they satisfy (5).

*ii) Computation of the linear stable–unstable spaces.* To compute numerical approximations of the linear space $E^u(x)$ we can now take advantage of the hyperbolicity of the dynamics. Precisely, we take a generic initial tangent vector $\xi = (\xi_{\varphi_1}, 0, \xi_{I_1}, 0) \in E^s(x) \oplus E^u(x)$ and we define the sequence:

$$\xi_k = D\phi^k(x)\xi = (\xi^k_{\varphi_1}, 0, \xi^k_{I_1}, 0) \in E^s(\phi^k(x)) \oplus E^u(\phi^k(x)) \quad .$$

The components $(\xi^k_{I_1}, \xi^k_{\varphi_1})$ do not necessarily converge to limit values, but we know from hyperbolicity that the component of $\xi_k$ on the space $E^u(\phi^k(x))$ expands exponentially with $k$, while the component of $\xi_k$ on the space $E^s(\phi^k(x))$ contracts exponentially with $k$. Therefore, if $k$ is a suitable high number (compared to the exponent of the expanding direction), the direction of the unstable space $E^u(\phi^k(x))$ is determined by $\xi_k$. For example, for the initial condition $(\varphi_1, \varphi_2, I_1, I_2) = (\pi, 0, 0, 0.324)$, $a = 0.4$, $\epsilon = 10^{-4}$, after $k = 10^5$ iterations we obtain:

$$x_k = \phi^k(x) \sim (\pi, 4.070625, 0, 0.324319) \ , \ \ E^u(x_k) \sim < (0.652, 0, 0.75749, 0) >$$

and $x_j = \phi^j(x), E^u(x_j)$ can be easily computed for any needed $j$.
A test of the precision reached by these computations is made by computing $E^u(x_{k'})$ for $k' > k$ and by analyzing the variation of the slope of $E^u(x_{k'})$ as $x_{k'}$ approaches $x_k$. Two computations are reported in figure 4: one for $k = 10^5$ as above, and another one for the small $k = 10$. The computation for $k = 10^5$ shows that the slope of $E^u(x_{k'})$ converges to the slope of $E^u(x_k)$ as $x_{k'}$ approaches $x_k$. This confirms that $k = 10^5$ is sufficient to compute the unstable space with an error smaller than $10^{-12}$, as it appears from figure 4. Moreover, because the data in figure 4 can be fitted by a straight line of slope 1, we can infer that $E^u(x)$ is compatible with a Lipschitz condition in a neighbourhood of $x$. In the figure we report for comparison the same computation for $k = 10$: in this case the slope of $E^u(x_{k'})$ does not converge to the slope of $E^u(x_k)$ as $x_{k'}$ approaches $x_k$, but the difference among the slopes converges to a quantity of order $10^{-6}$.

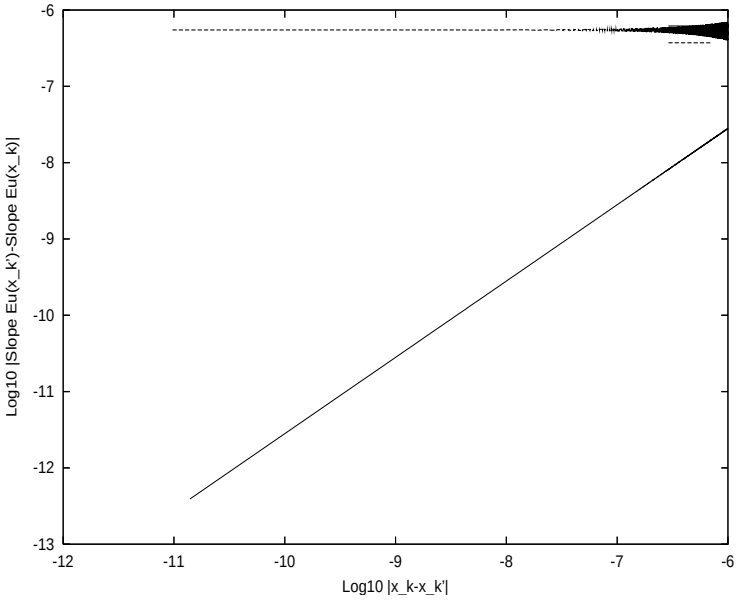


**Fig. 4.** Test of the numerical precision in the computation of $E^u(x_k)$. The figure reports in logarithmic scale the difference among the slope of $E^u(x_{k'})$ and the slope of $E^u(x_k)$ (on the $y$ axis) versus $|x_k - x_{k'}|$ (on the $x$ axis), for those $k' > k$ such that $|x_k - x_{k'}| \leq 10^{-6}$. The upper curve refers to the case $k = 10$, which provides poor precision of the computation (of order $10^{-6}$), the lower curve refers to the case $k = 10^5$, which provides good precision (better than $10^{-12}$). The data for $k = 10^5$ can be fitted by a straight line of slope 1. We can therefore infer that, within this precision, $E^u(x)$ is compatible with a Lipschitz condition in a neighbourhood of $x$.

*iii) Computation of the stable–unstable manifolds.* For any point $x_j$, denoting by $\xi_j$ the unit vector generating the unstable space $E^u(x_j)$, we use the linear approximation:

$$W^{loc}(x_j) \sim \{x_j + s\ \xi_j \quad , \quad s \in [0, \rho)\} \quad , \tag{13}$$

which is good as soon as $\rho$ is very small (we use $\rho = 10^{-10}$ in our computations).

Then, we compute finite pieces of the unstable manifold using:

$$\phi^j(W_u^{loc}(x_{-j})) \subseteq W_u(x) \quad .$$

The small errors done by using the linear approximation for the local manifold do not accumulate at successive iterations, because the hyperbolic dynamics tends to reduce them (see [28]). Being interested also in computing a parametrization of the manifold with respect to its arc length, we proceed in two steps. First, we set $K$ such that:

$$W_K(x) = \cup_{j=1}^{K} \phi^j(W_u^{loc}(x_{-j})) \subseteq W_u(x) \tag{14}$$

can be parametrized by the $\varphi_1$ coordinate, so that we can order the points in $W_K(x)$ with respect to $\varphi_1$ (figure 5, left). This allows one to construct a

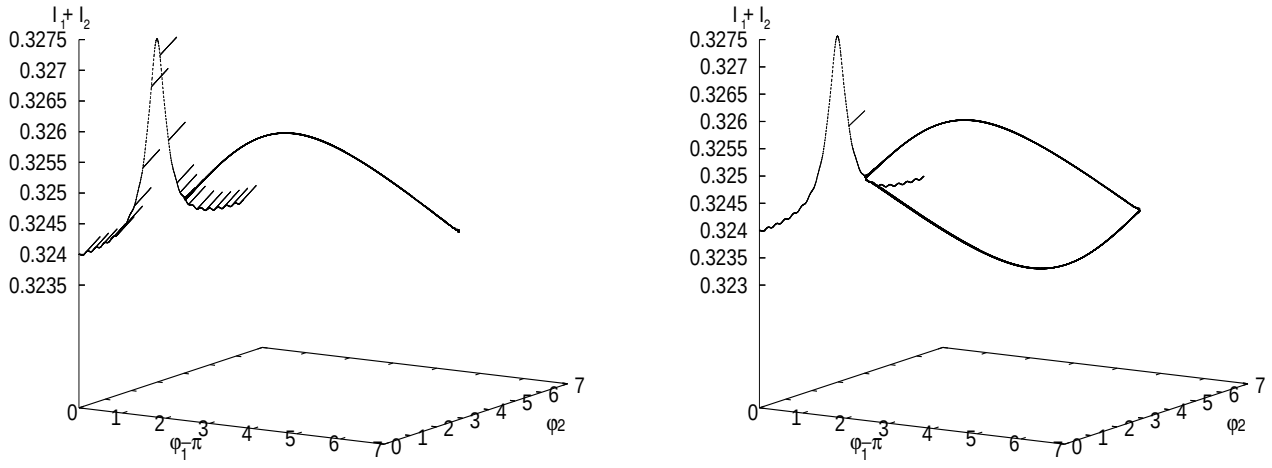


**Fig. 5.** Sketch of the first (left panel) and second (right panel) step of the algorithm of computation of the unstable manifold. The coordinates of the plot are: ($\varphi_1 - \pi$, $\varphi_2$,$I_1 + I_2$). One invariant torus of the map restricted to $\Lambda$ is plotted. We recall that $\varphi_1 = \pi$ and $I_1 = 0$ on $\Lambda$. (Left panel) The segments correspond to the local linear approximation of the unstable manifold of the points $x_{-j}$, $j = 1, ...K$. The flow $\phi^j$ applied on such points allows one to construct $W_K(x)$ (the "arc-shaped" structure), with $x$ selected in $\Lambda$ as explained in the text. (Right panel) Some of the points $x_{-K}$ are plotted (the segment in the picture). The flow $\phi^K$ allows one to add ordered points to the manifold $W_u(x)$. In order to have a uniform sampling of the manifold with respect to its arc length the choice of the points $x_{-K}$ is adapted to the evolution of the arc parameter of the manifold as explained in the text.

parametrization of $W_K(x)$ with respect to its arc–length, that we denote by:

$$s \longmapsto (\varphi_1(s), \varphi_2(s), I_1(s), I_2(s)) \quad .$$

Then, we want to reconstruct the unstable manifold also for an arc–length much longer than the one obtained at the first step, so that to include many lobes of the manifold. This can be easily done by mapping with $\phi^K$ additional points of the linear approximation of the local manifold (figure 5, right panel), but paying attention to obtain a uniform sampling of the manifold with respect to its arc–length. This problem was already discussed in [28] and we use a similar procedure for the choice of the initial conditions on $W_u^{loc}(x_{-K})$. More precisely, let us denote by $x^m, x^{m+1}$ the last two points of $W_u^{loc}(x_{-K})$ used to compute $W_K(x)$, by $\Delta x^m = d(x^m, x^{m+1})$, and by $\Delta s^m = s^{m+1} - s^m$ the difference of the arc–lengths of the points $\phi^K(x^m)$,$\phi^K(x^{m+1})$. The choice of the point $x^{m+2}$ will be done depending on $\Delta s^m$ as follows:

$$\begin{cases} x^{m+2} = x^{m+1} + \Delta x^m & \text{if } \Delta s_1 < \Delta s^m < \Delta s \\ x^{m+2} = x^{m+1} + \eta \Delta x^m & \text{if } \quad \Delta s^m > \Delta s \\ x^{m+2} = x^{m+1} + \frac{1}{\eta} \Delta x^m & \text{if } \quad \Delta s^m < \Delta s_1 \end{cases} \tag{15}$$

with $\Delta s = 10^{-2}$, $\Delta s_1 = 10^{-3}$ and $\eta = 0.1$.

**2) Detection of stable manifolds using the Fast Lyapunov Indicator**

We have found a new application of the FLI method which allows one to obtain a sharp detection of the intersection of the stable and unstable manifolds of the normally hyperbolic invariant manifolds with any two dimensional surface of the phase–space.

In the last years the so called fast Lyapunov indicator [10] has been extensively used to numerically detect the phase space structure, i.e. the distribution of KAM tori and resonances, of quasi–integrable systems [11], [12],[14]. For a map $\psi : M \to M$, the simplest definition of fast Lyapunov indicator of a point $x \in M$ and of a tangent vector $v \in T_x M$, at time $t$, is:

$$\mathrm{FLI}_t(x, v) = \log\left(\frac{\|v_t\|}{\|v\|}\right) \quad , \tag{16}$$

where $v_t = D^t\psi(x)v$. The infinite limit $\lim_{t\to\infty} \mathrm{FLI}_t(x, v)/t$ provides the Lyapunov exponent of the point $x$ and vector $v$. But, $\mathrm{FLI}_t(x, v)$ provides informations about the dynamics of the orbit of initial condition $x$ already on finite times $t$: in the papers [11], [12],[14] it is shown that, for quasi–integrable systems, if $t$ is suitably long (precisely of some inverse power of the perturbing parameter, see [14] for precise statements and proofs) the value of $\mathrm{FLI}_t(x, v)$ is different, at order 0 in $\epsilon$, in the case $x$ belongs to an invariant KAM torus from the case $x$ belongs to a resonance of the system. Therefore, the computation of $\mathrm{FLI}_t(x, v)$ on grids of initial conditions $x \in M$ and a fixed vector $v$ allows one to detect the distribution of invariant tori and resonances in relatively short CPU times ([11], [12]).

In this paper we make a different use of the fast Lyapunov indicator to detect stable and unstable manifolds of invariant hyperbolic manifolds. The principle is the following. We sample two dimensional surfaces of the phase space with grids of points. For any point $x$ of the grid and the same vector $v$ we compute the $\mathrm{FLI}_T(x, v)$ for some time $T$. The points of the grid which will have the highest values of the FLI are those points whose orbits approach an hyperbolic invariant manifold within the time $T$, because the growth of tangent vectors is bigger near the hyperbolic manifolds. Therefore, a short–time computation of the FLI allows one to detect a neighborhood of a finite piece of the stable manifold (the unstable manifold can be obtained by computing the FLI of the inverse map). As a check on a well known example, we compare in figure 6 the computation of finite pieces of the unstable manifold of the hyperbolic fixed point of the standard map:

$$\varphi' = \varphi + I \quad , \quad I' = I - a\sin\varphi' \tag{17}$$

with $a = 0.4$. In the left panel we report the computation of finite pieces of the unstable manifold in a neighbourhood of the fixed point obtained by using the traditional method of propagation of sets of points. In the right panel we report the computation of the FLI of inverse map for a grid of points in the same neighbourhood of the fixed point. The light gray lines in the right panel[1] represent the points of the grid with the highest value of the FLI, and they clearly correspond to pieces of the unstable manifold.

[1] The color version of all figures can be found on the electronic version of the paper so that light gray corresponds there to yellow and darker gray corresponds there to darker orange.

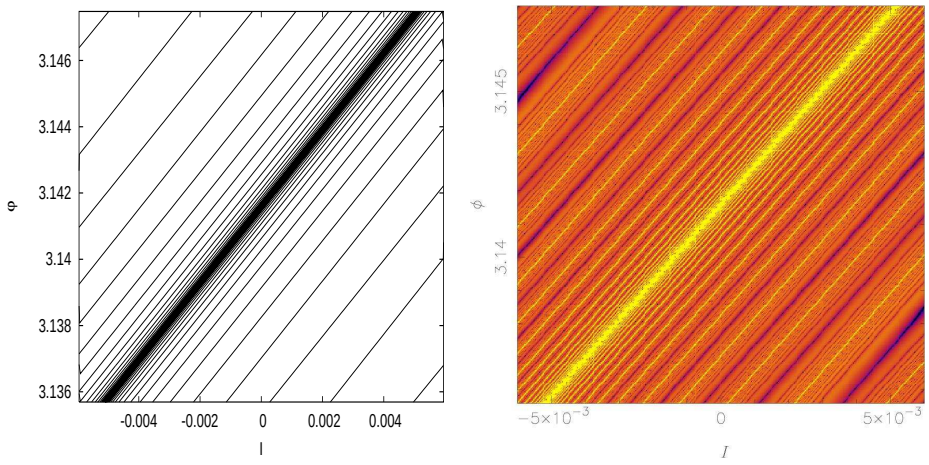


**Fig. 6.** Detection of a piece of the unstable manifold of the standard map (17) in the neighbourhood of the hyperbolic fixed point $\varphi \in [\pi - 0.006, \pi + 0.006]$, $I \in [-0.006, 0.006]$. **On the left:** Detection of the manifold with the traditional method of propagation of sets. **On the right:** Detection of the manifold with the FLI method. The FLI has been computed using the inverse of the standard map (17), a set of $500 \times 500$ initial conditions, a maximum of $T = 40$ iterations of the map. The color scale range is such that FLI$> 3.3$ is represented by light gray color (darker grays correspond to lower values of the FLI).

The agreement among the results of the two methods is good and in particular we remark the sharpness of the detection of the stable manifold with the FLI method. The application of the FLI method to higher dimensional systems is nearly as simple as in this two dimensional case, and one does not need to know in advance which are the normally hyperbolic invariant manifolds and their local approximations. In fact, the method detects the stable manifolds of all the hyperbolic structures of the system.

The application of this method to the detection of stable manifolds in more complicate examples, such as the map (10), is described in the next section.

## 5. Topology of the stable and unstable manifolds of $\Lambda$

In this section we compute different representations of the stable and unstable manifolds of $\Lambda$ for $a > 0$. When $\epsilon = 0$ the stable and unstable manifolds $W_s, W_u$ of $\Lambda$ are the product of the stable and unstable manifolds $W_s^*, W_u^*$ of the hyperbolic fixed point of the standard map:

$$\varphi_1' = \varphi_1 + I_1 \quad , \quad I_1' = I_1 - a \sin \varphi_1' \tag{18}$$

with the cylinder $\mathbb{R} \times \mathbb{T}$, domain of $(I_2, \varphi_2)$; $W_s$ intersects $W_u$ at any intersection point of $W_s^*, W_u^*$; $I_2$ is constant of motion.

To study diffusion along $\Lambda$ and to represent the manifolds $W_s, W_u$ we consider the two dimensional surface of the phase–space:

$$S = \{(\varphi_1, \varphi_2, I_1, I_2) \ \text{ such that } : \varphi_1 = \pi \quad , \quad \varphi_2 = 0\} \quad , \tag{19}$$

so that in the following we describe and compute the topology of the sets:

$$S_u^* = S \cap W_u \quad , \quad S_s^* = S \cap W_s \quad .$$

Any invariant torus of $\phi_{|\Lambda}$ intersects $S_u^*$ in only one point, so that $S_u^*$ is the set where points with initial conditions in a neighborhood of $S$ can return near $S$ following diffusion paths defined by the unstable manifolds of the points of $\Lambda$. When $\epsilon = 0$ it is:

$$S_u^* = \{(\varphi_1, \varphi_2, I_1, I_2) \ \text{ such that : } \ (I_1, \pi) \in W_u^* \ , \ \varphi_2 = 0\} \ ,$$

that is a set of lines parallel to the $I_2$ axis. The same holds for $S_s^*$. When $\epsilon \neq 0$ understanding the topology of $S_u^*, S_s^*$ becomes a difficult problem, but if $\epsilon$ is very small, we can use Melnikov like approximations.

**A Melnikov–like approximation of $S_u^*$**

The Melnikov approximations of a priori unstable systems are obtained by neglecting the perturbation on the hyperbolic part of the system, which is usually chosen to be integrable by quadratures. Here, the unperturbed hyperbolic part of the system is represented by the standard map (18), which is not integrable. Nevertheless, we define a Melnikov–like approximation:

**Definition.** *Let us consider $x = (\varphi_1, \varphi_2, I_1, I_2) \in \Lambda$ and denote $J = I_2$. We define the Melnikov approximation of $W_u(x)$ to be the unstable manifold of $x$ with respect to the following simplified map $\tilde{\phi}$:*

$$\begin{aligned} \varphi_1' &= \varphi_1 + I_1 \quad & \varphi_2' &= \varphi_2 + J \\ I_1' &= I_1 - a \sin \varphi_1' \quad & I_2' &= I_2 + \epsilon \frac{\sin \varphi_2'}{(\cos \varphi_1' + \cos \varphi_2' + c)^2} \end{aligned} \quad . \tag{20}$$

We can represent the Melnikov approximation of $W_u(x)$ as follows:

**Proposition.** *Let us consider $x = (\tilde{\varphi}_1, \tilde{\varphi}_2, \tilde{I}_1, \tilde{I}_2) \in \Lambda$ and denote $J = \tilde{I}_2$. The Melnikov approximation of $W_u(x)$ is represented by all points $z = (\varphi_1, \varphi_2, I_1, I_2)$ such that $(\varphi_1, I_1)$ is in the unstable manifold $W_u^*$ of the fixed point $(\pi, 0)$ with respect to the map:*

$$\varphi_1' = \varphi_1 + I_1 \quad , \quad I_1' = I_1 - a \sin \varphi_1' \quad , \tag{21}$$

*while $\varphi_2 = \tilde{\varphi}_2$ and:*

$$I_2 = \tilde{I}_2 - \epsilon \sum_{k=-1}^{-\infty} \Big( \frac{\sin(\tilde{\varphi}_2 - kJ)}{(\cos \varphi_1(k) + \cos(\tilde{\varphi}_2 - kJ) + c)^2} - \frac{\sin(\tilde{\varphi}_2 - kJ)}{(\cos(\tilde{\varphi}_2 - kJ) + c - 1)^2} \Big) \tag{22}$$

*where $(\varphi_1(j), I_1(j))$ denote the orbit with initial condition $(\varphi_1, I_1) \in W_u^*$ with respect to the map (21).*

The proof of this proposition is reported at the end of this section. Here, we use the proposition to obtain a parametric representation of the unstable manifolds in the Melnikov approximation. In figure 7 we compare two parametrizations $s \mapsto (I_2(s) - I_2(0))$ of the manifold $W_u(x)$: one is obtained with the Melnikov approximation (22), while the other one is obtained using the full map and the

method described in section 4. The left panel shows that for $\epsilon = 10^{-6}$ the two parametrizations are indeed very close one to the other. The right panel shows that for $\epsilon = 10^{-4}$ the Melnikov approximation is no valid at all.

In order to appreciate the accuracy of the Melnikov approximation we have computed for $10^{-8} < \epsilon < 10^{-3}$ the histogram of $(I_2(s) - I_2(0))/\epsilon$ for both the full map and the Melnikov approximation. We consider as an indicator of the distance between the two distributions the quantity:

$$d = \frac{\sum_{i=1}^{N}(H_f(i) - H_M(i))^2}{N} \tag{23}$$

where $H_f$ and $H_M$ correspond to the histograms of $(I_2(s) - I_2(0))/\epsilon$ for respectively the full map and the Melnikov approximation and $N = 100$ is the number of bins. The quantity $d$ (figure 7) remains smaller than $3\,10^{-6}$ up to $\epsilon = 5\,10^{-6}$ and suddenly increases with $\epsilon$, although not regularly, for higher values of the perturbing parameter. We remark that the transition value $5\,10^{-6}$ is close to the transition value from a regular to an irregular behavior of the diffusion coefficient (figure 2).

In order to describe the topology of $S_u^*$ using the Melnikov approximation, we define the sequence $s_k$, $k \in \mathbb{N}$, such that $\varphi_1(s_k) = \pi$, so that the Melnikov approximation of $S_u^*$ is:

$$S_u^* = \cup_{k\in\mathbb{N}}(\varphi_1(s_k), 0, I_1(s_k), I_2(s_k)) \quad ,$$

that is a set of lines parallel to the $I_2$ axis, as in the unperturbed case. As a consequence, when the topology of finite pieces of $S^*$ is very far from lines parallel to the $I_2$ axis, the system is very far from the validity of the Melnikov approximation regime. We describe below the detection of a transition in the topology of the sets $S_u^*, S_s^*$ which turns out to correspond to the loose of validity of the Melnikov approximation.

**A transition in the topology of $S_s^*$, $S_u^*$**

We considered the map (10) with $c = 2.1$, $a = 0.4$ and we computed $S_s^*$ for different values of $\epsilon$ by computing the FLI on refined grids of $1000\times1000$ regularly spaced points of $S$. The results are shown in figures[2] 9,10: the three columns of the figures represent different zooms of $S$ with respect to the action $I_1$, allowing one to appreciate the topology of $S_s^*$ from the small values of $I_1 \in [10^{-11}, 10^{-8}]$ (left column) up to $I_1$ of order 0.1 (right column). Each line refers to a different value of $\epsilon$, so that we can appreciate the evolution of $S_s^*$ from $\epsilon = 0$ up to $\epsilon$ of order $10^{-3}$. The action $I_2$ is in the range $[0, 1]$. We now comment the results. For $\epsilon = 0$ (top line of figure 9) we recognize that $S_s^*$ is a set of lines parallel to the axis $I_1 = 0$ with accumulation towards $I_1 = 0$, as we expected. For $\epsilon = 10^{-6}$ (second line of figure 9) the situation is very similar to the case with $\epsilon = 0$: $S_s^*$ seems to be represented by vertical lines (of course with small deviations), as it is expected if the Melnikov approximation is valid. For $\epsilon = 6\ 10^{-6}$ (last line of figure 9) most of the vertical lines are still visible in the three zooms, though with an evident distortion. However, the vertical lines have disappeared in some

[2] To better appreciate the topology we uploaded high resolution pictures available at *http://www.obs-nice.fr/elena/topology/figcolor.tar.gz*. In the final version of the paper the high resolution pictures will be used.

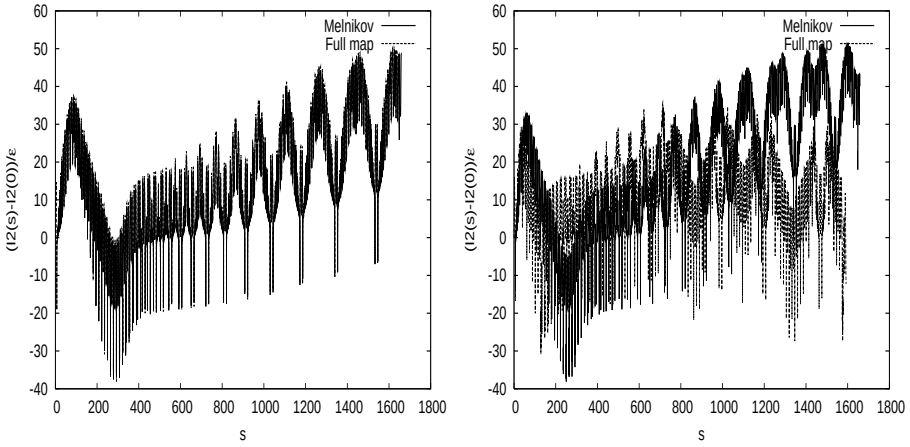


**Fig. 7.** Each panel represents two parametrizations $s \mapsto (I_2(s) - I_2(0))/\epsilon$ of the manifold $W_u(x)$, with $x = \phi^{10^5}(\pi, 0, 0, 0.324)$ : one is obtained using the Melnikov approximation, while the other one is obtained using the full map. The left panel is for $\epsilon = 10^{-6}$: the two parametrizations are close one to the other. The right panel is for $\epsilon = 10^{-4}$: the Melnikov approximation is not valid.

regions. For $\epsilon = 4\ 10^{-5}$ (top line of figure 10) we are close to a transition in the topology of all vertical lines, which becomes more evident for $\epsilon = 6\ 10^{-5}$ (second line of figure 10), where horizontal lines appear. This kind of topology cannot be explained by the Melnikov approximation, which is therefore not valid for this value of $\epsilon$. For $\epsilon = 6\ 10^{-4}$ (last line of figure 10) the transition in the topology of $S_s^*$ is complete: the inner zoom shows only horizontal lines and also the outer zoom reveals a topology which is completely different from the one which is expected in the Melnikov approximation. We say that for this value of $\epsilon$ the transition of the topology of $S_s^*$ in the range of $I_2 \in [0, 1]$ is completed.

We repeated these computations for $I_2 \in [1.4, 2.4]$, and we detected the same kind of transitions in the topology of $S_s^*$.

Summarizing these results, we have shown that for small values of $\epsilon$ the topology of $S_s^*$ is consistent with the description of the stable (unstable) manifolds obtained with the Melnikov approximation, i.e. it is characterized by the prevalence of vertical lines. For high values of $\epsilon$ the topology is characterized by horizontal lines which originate at the resonances on $\Lambda$. This happens even for values of $\epsilon$ such that the restricted map has still al lot of invariant tori. For intermediate values of $\epsilon$ we detect a transition among the two topologies, in which the vertical lines are distorted up to be completely replaced by horizontal lines.

We find useful to compare the different topologies of $S_s^*$ with the dependence of the diffusion coefficient on $\epsilon$ represented in figure 2, where we identified a law for the diffusion coefficient $D \sim \epsilon^2$ for $\epsilon < \epsilon_1 \sim 6\ 10^{-6}$, some irregular behavior up to $\epsilon = \epsilon_2 \sim 4\ 10^{-4}$, and a different regular power law for $\epsilon > \epsilon_2$. We remark that the interval $(\epsilon_1, \epsilon_2)$ corresponds approximately to the interval of transition from the topology characteristic of the Melnikov approximation to the completely different topology characterized by the horizontal structures, so

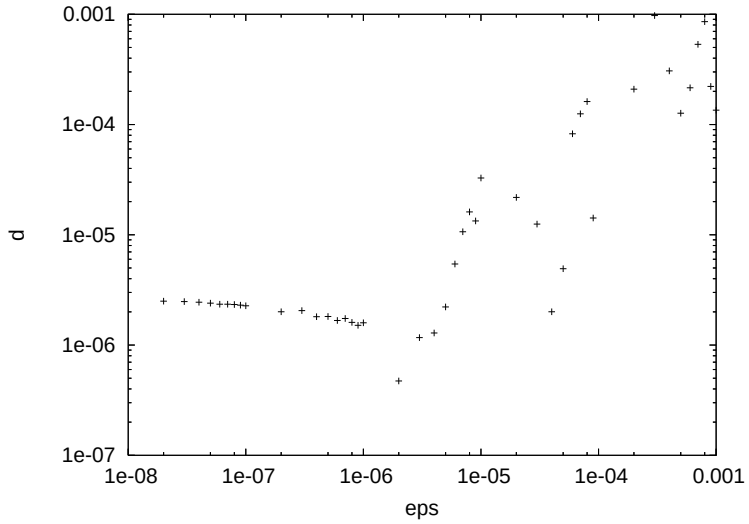


**Fig. 8.** Computation of $d$ defined in (23) as a function of $\epsilon$. We can appreciate that $d$ remains smaller than $3\,10^{-6}$ up to $\epsilon = 5\,10^{-6}$. For higher values of the perturbing parameter $d$ suddenly increases with $\epsilon$, although not regularly.

that the topology of the stable (unstable) manifold and the dependence of the diffusion coefficient on $\epsilon$ are correlated.

### Proof of the Proposition

Let us denote by $z(j) = (\varphi_1(j), \varphi_2(j), I_1(j), I_2(j))$ the orbit of $z = z(0) = (\varphi_1, \varphi_2, I_1, I_2)$ and by $x(j) = (\tilde{\varphi}_1(j), \tilde{\varphi}_2(j), \tilde{I}_1(j), \tilde{I}_2(j))$ the orbit of $x = \tilde{x}(0) = (\tilde{\varphi}_1, \tilde{\varphi}_2, \tilde{I}_1, \tilde{I}_2)$ with respect to the map $\tilde{\phi}$. The point $z$ is in the unstable manifold of $x$ if and only if it is:

$$\lim_{j \to -\infty} \|z(j) - x(j)\| = 0 \quad .$$

Therefore, $(I_1(j), \varphi_1(j))$ tends to $(0, \pi)$ as $j \to -\infty$ if and only if $(I_1(0), \varphi_1(0))$ is in the unstable manifold $W^u$ of the fixed point $(\pi, 0)$ with respect to the map (21). Let us now prove (22). For any $j \leq -1$ it holds:

$$I_2(j) = \sum_{k=-1}^{j} (I_2(k) - I_2(k+1)) + I_2(0) = \epsilon \sum_{k=-1}^{j} \frac{\sin \varphi_2(k+1)}{(\cos \varphi_1(k+1) + \cos \varphi_2(k+1) + c)^2} + I_2 \quad ,$$

as well as:

$$\tilde{I}_2(j) = \sum_{k=-1}^{j} (\tilde{I}_2(k) - \tilde{I}_2(k+1)) + \tilde{I}_2(0) = \epsilon \sum_{k=-1}^{j} \frac{\sin \tilde{\varphi}_2(k+1)}{(\cos \tilde{\varphi}_2(k+1) + c - 1)^2} + \tilde{I}_2 \quad .$$

Therefore, it is:

$$\lim_{j \to -\infty} \|I_2(j) - \tilde{I}_2(j)\| = 0$$

if and only if (22) holds.

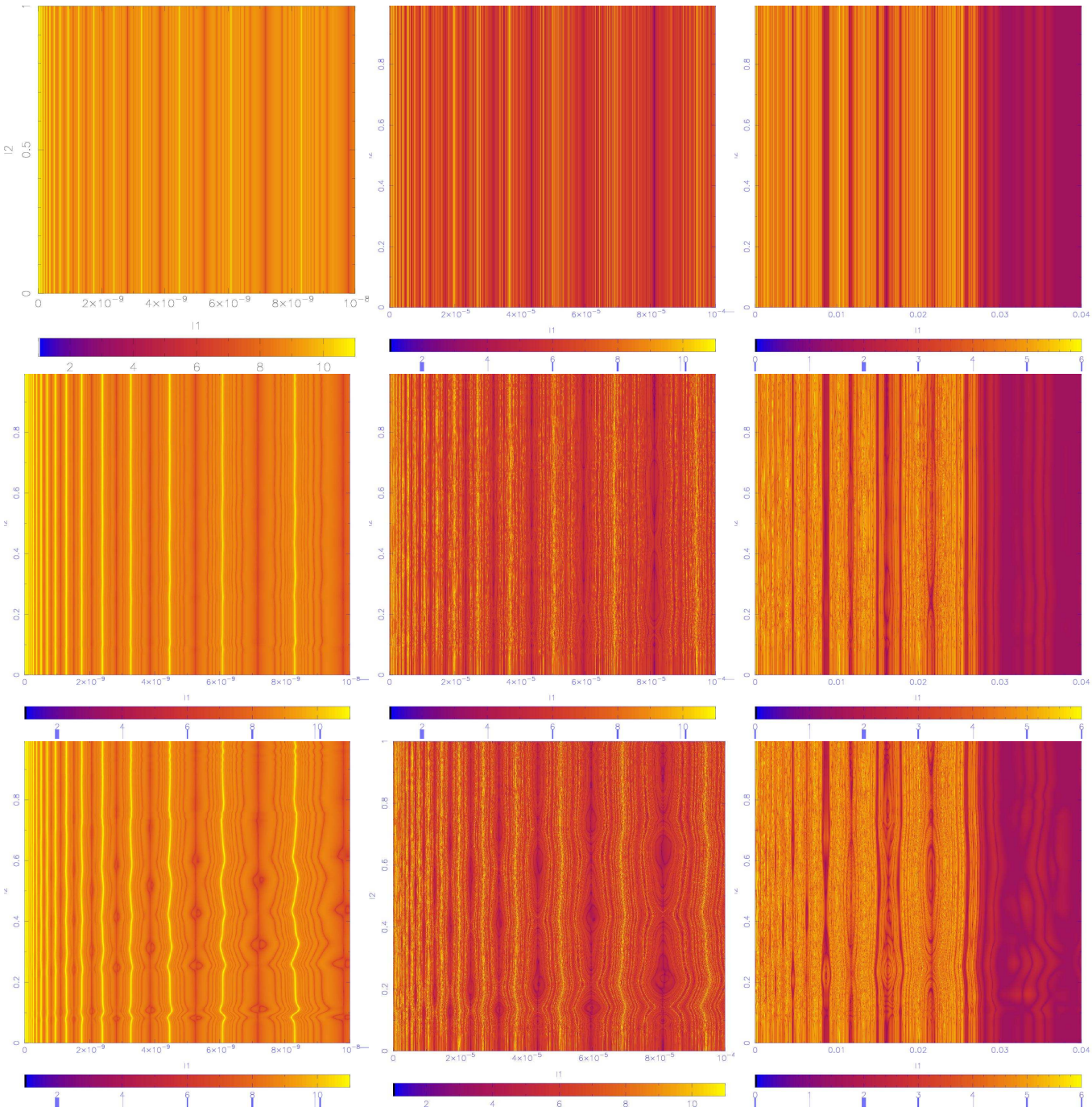

**Fig. 9.** Computation of $S_s^*$ for $I_1 < 10^{-8}$ ($T = 60$, left panels), for $I_1 < 10^{-4}$ ($T = 80$, middle panels) and $I_1 < 10^{-2}$ ($T = 80$, right panels). The perturbation is (from top to bottom) $\epsilon = 0, 10^{-6}, 6\ 10^{-6}$. The light gray lines correspond to finite pieces of the stable manifold.

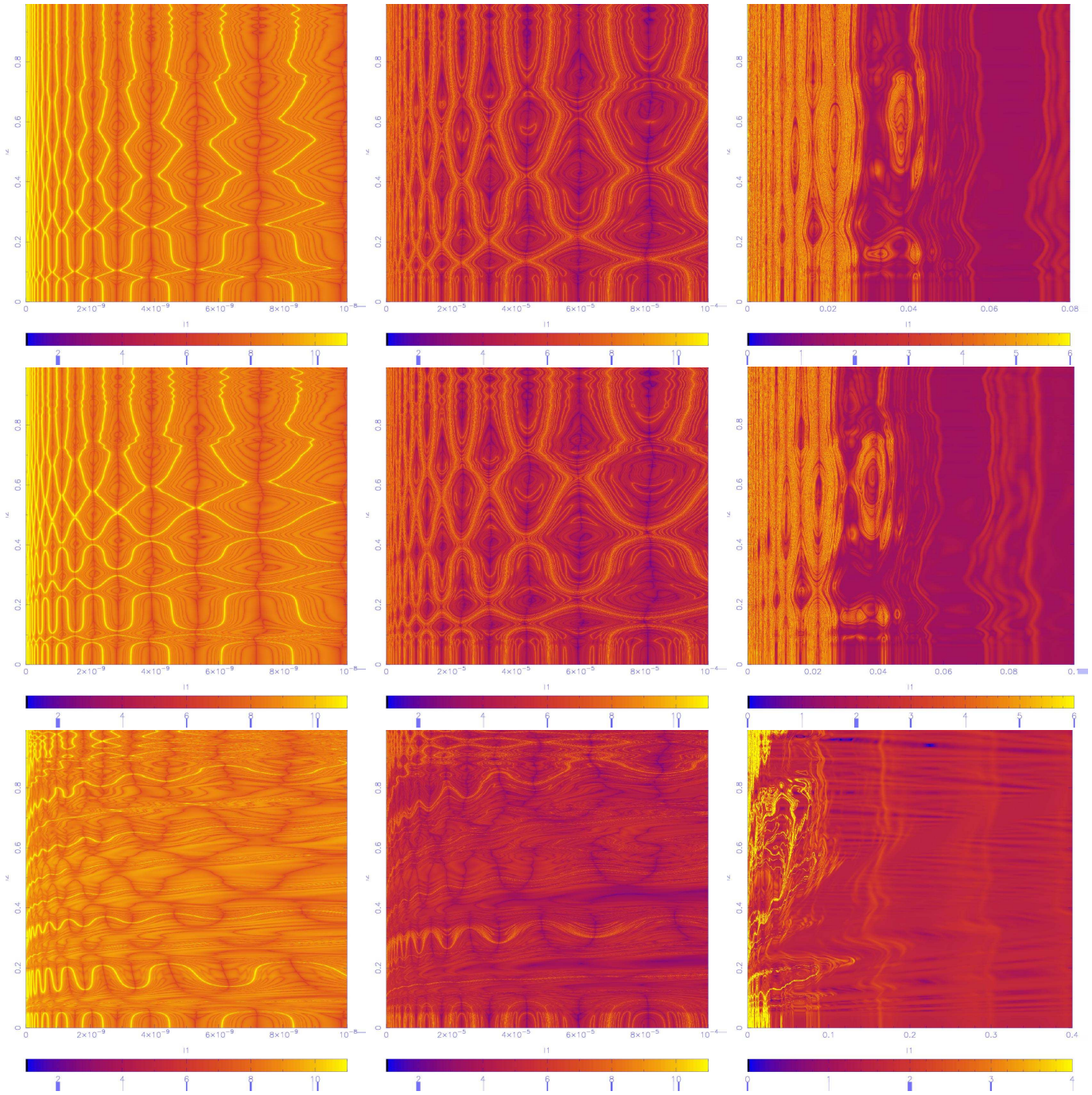

**Fig. 10.** Computation of $S_s^*$ for $I_1 < 10^{-8}$ ($T = 60$, left panels), for $I_1 < 10^{-4}$ ($T = 80$, middle panels) and $I_1 < 10^{-2}$ ($T = 80$, right panels). The perturbation is (from top to bottom) $\epsilon = 4\ 10^{-5}, 6\ 10^{-5}, 6\ 10^{-4}$. The light gray lines correspond to finite pieces of the stable manifold.

## 6. Spread of the unstable manifolds and diffusion

We computed the parametrization of $W_u(x)$ using the first method reported in section 4 for quite a long arc–length for different values of $0 < \epsilon < \epsilon_c$ ($a = 0.4$, $c = 2.1$) and for different types of orbits of $\phi_{|\Lambda}$, KAM tori, regular resonant librations and resonant chaotic motions.

In figures 12, 13, 14 (top right panels) it appears clearly that $I_2(s)$ undergoes large fluctuations for all the kind of different dynamics. The unstable manifolds, which are contained in a plane of constant $I_2$ for $\epsilon = 0$, are unrolled along the $I_2$ direction for $\epsilon > 0$, thus supporting diffusion in the neighborhood of $\Lambda$. To appreciate that the manifolds are unrolled in the phase–space we represent them (bottom right panels) in the three–dimensional space $\varphi_1, I_1, I_2$. The reference orbits of the restricted map are represented in the bottom left panels. To measure the spread of the manifolds in the $I_2$ direction we also plot on the bottom left panels the vertical segments which correspond to the representation on the plane $(I_2, \varphi_2)$ of the points of $W_u(x)$ with $|\varphi_1 - \pi| \leq 0.5$ (reducing the tolerance on $\varphi_1$ decreases the number of points on the figure, but does not decrease the amplitude of the segment). For the case of the KAM torus (figure 12) for $\epsilon = 10^{-6}$ this segment is definitely bigger than the variation of $I_2$ along the torus.

To show that the spread of the unstable manifold is compatible with the numerical Arnold diffusion stated in (v) we computed the evolution of points in the unstable manifold $W_u^{loc}(x')$, with $x' = \phi^{10^3}(\pi, 0, 0, 0.324)$ and $\epsilon = 10^{-6}, 10^{-4}$, with the high numerical precision of 400 digits, and we check if some points of the integrated orbits are good candidates to satisfy condition (2). For both $\epsilon = 10^{-6}, 10^{-4}$ the point $x'$ belongs to an invariant torus.

We remark that the quantity $|\Delta I_2'|$ is negligible with respect to $c_2$ for $\epsilon = 10^{-6}$ or $\epsilon = 10^{-4}$, because the $I_2$ component of $E^u(x')$ is 0 and $|\Delta x'| \leq 10^{-10}$ for all the points in $W_u^{loc}(x')$.

For the first computation, with $\epsilon = 10^{-6}$, the amplitude of the torus containing $x'$ with respect to the action $I_2$ is approximately $3\ 10^{-5}$, and the constant $c_2$ for the set $\tilde{\Lambda}$ defined by $|I_2 - 0.324| \leq 4\ 10^{-4}$ can be set to $c_2 = 4\ 10^{-5}$. We find that condition (2) is satisfied with a $\Delta x''$ characterized by $|\Delta I_2''| \sim 10^{-12}$ (see figure 11, top–right panel) and $x'' = (\pi, 0, 5.500622..., 0.3243360129...)$. Using the notation of section 1, for any $(\tilde{I}', \tilde{\varphi}') \in \mathcal{C}(x')$, $(\tilde{I}'', \tilde{\varphi}'') \in \mathcal{C}(x'')$ it is (see figure 11, top–left panel):

$$\left| \tilde{I}_2' - \tilde{I}_2'' \right| > 2.6\ 10^{-4} > 6\ c_2 \quad , \tag{24}$$

that is condition (2) is satisfied. Moreover, the numerical precision $\rho$ of the computation is estimated to be smaller than $10^{-173}$, so that also (3) is satisfied. The error estimator $\rho$ is computed as follows. We consider a set of 10 points in a segment of amplitude $\lambda = 10^{-N}$ aligned to $E^u(x')$, in a neighbourhood of $x' + \Delta x'$. Then, we computed the orbits of these 10 points for the number of iterations $T$ such that $\phi^T(x' + \Delta x') + \Delta x'' \in W_s(x'')$ with a numerical precision of $2N$. We decide that $N$ is sufficiently large, compared to $T$, when the map $\phi$ separates the 10 points of a quantity $\rho$ which is much smaller than the precision required to verify equation (2). For example, in this case $T = 1382$, we found

that $\rho < 10^{-93}$ for $N = 120$, $\rho < 10^{-153}$ for $N = 180$, while $\rho = 10^{-173}$ with the actual precision of 400 digits.

For the second computation, with $\epsilon = 10^{-4}$, the amplitude of the torus containing $x'$ with respect to the action $I_2$ is approximately $4\ 10^{-3}$, and the constant $c_2$ for the set $\tilde{\Lambda}$ defined by $I_2 \in [0.3239, 0.3388]$ can be set to $c_2 = 4\ 10^{-3}$ as well. We found that condition (2) is satisfied for $x'' = (\pi, 0, 2.823858..., 0.3387504482...)$, that is:

$$\left|\tilde{I}'_2 - \tilde{I}''_2\right| > 7\ 10^{-3} > 1.6\ c_2 \quad , \tag{25}$$

while $|\Delta I''_2| < 10^{-7}$ (see figure 11, bottom–right panel). We remark (see figure 11, bottom–left panel) the presence of a large resonance between the invariant tori containing $x'$ and $x''$, and therefore the unstable manifold of $x'$ has crossed this large gap before arriving near the stable manifold of $x''$. The numerical precision $\rho$ of the computation is estimated to be smaller than $10^{-113}$, so that also (3) is satisfied. The error estimator $\rho$ is computed as explained above: in the case $T = 1951$, we found that $\rho < 10^{-33}$ for $N = 120$, $\rho < 10^{-93}$ for $N = 180$, and $\rho < 10^{-113}$ for the actual precision of 400 digits.

We computed also the spread of the unstable manifold of points which are on a resonant regular libration and a chaotic orbit, for $\epsilon = 10^{-4}$ (figures 13, 14). The amplitudes of the segments representative of the spread of $W_u(x)$ along the $I_2$ direction are $2\ 10^{-3}$, $1.5\ 10^{-3}$ respectively.

We remark that all these conclusions are obtained for a value of $\epsilon$ for which the Melnikov approximation is valid ($\epsilon = 10^{-6}$) as well as for a value for which the Melnikov approximation is not valid, but the dynamics of $\phi_{|\Lambda}$ is still characterized by many invariant tori.

From figures 12, 13, 14, we observed that the unstable manifolds are characterized by many oscillations in the $I_2$ direction which remind us of the oscillation that the actions do in diffusing along the resonances. Therefore, to remove the effect of the oscillations and to look for a systematic spread of the manifolds in the $I_2$ direction we compute the quadratic averages of the quantity $I_2(s) - I_2(0)$ with respect to many close initial points $x$. In figure 15 we represented:

$$d(s) = \frac{1}{N} \sum_{j=1}^{N} \left( I_2^j(s) - I_2^j(0) \right)^2 \tag{26}$$

versus $s$ for $\epsilon = 10^{-5}$ ($N = 200$, the initial conditions are $I_1 = 0$, $\varphi_1 = \pi$, $0.6 < I_2 < 1$, $\varphi_2 = 0$). The figures present a systematic growth of the quadratic spread of the manifolds. The large oscillations are due to the excursions of $I_2$ with respect to $\varphi_1$. We can reduce them both computing a running average on eq. (26), or considering only the values $I_2(s)$ with $\varphi_1(s)$ in a suitable small interval as shown in figure 15, left panel. Finally, to provide a quantitative measure of the link between diffusion of orbits and geometric spread of the unstable manifolds we define a "geometrical" diffusion coefficient of the unstable manifolds. For this purpose, if we consider the restriction of the map $\phi$ to the unstable manifold, the arc–length $s$ grows nearly exponentially with time when the manifold passes near the hyperbolic invariant manifold. Denoting by $\lambda$ the mean value of the Lyapunov exponent computed over a time of $t = 10^9$ iterations (for a set of $N = 20$ orbits with initial conditions: $-10^{-5} < I_1 < 10^{-5}$, $\varphi_1 = \pi$, $0.3 < I_2 < 3$,

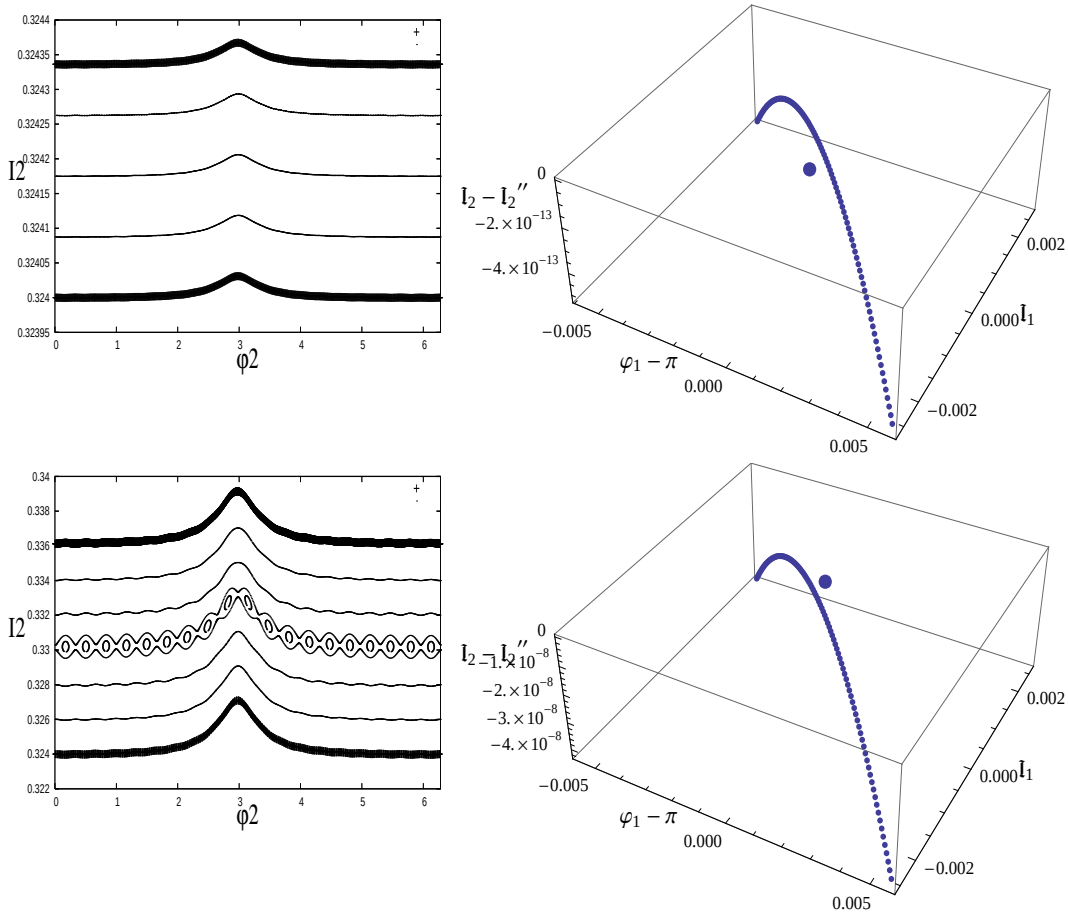


**Fig. 11.** Numerical test of equation (2). **On the top–left.** Phase plane of the map $\phi$ restricted to $\Lambda$ for $\epsilon = 10^{-6}$: the invariant tori containing $x'$ and $x''$ are represented by bold curves. **On the top–right.** Projection on the space of variables $\varphi_1 - \pi, I_1, I_2 - I_2''$ of the point $\phi^T(x' + \Delta x')$ in the orbit of $x' + \Delta x'$ and of the stable manifold of $x''$, for $\epsilon = 10^{-6}$. We remark that with a correction $\Delta x''$ characterized by $\Delta I_2''$ of order $10^{-13}$ the point $\phi^T(x' + \Delta x') + \Delta x''$ belongs to the stable manifold of $x''$. **On the bottom–left.** Phase plane of the map $\phi$ restricted to $\Lambda$ for $\epsilon = 10^{-4}$: the invariant tori containing $x'$ and $x''$ are represented by bold curves. We remark the presence of a large resonance between the two invariant tori. **On the bottom–right.** Projection on the space of variables $\varphi_1 - \pi, I_1, I_2 - I_2''$ of the point $\phi^T(x' + \Delta x')$ in the orbit of $x' + \Delta x'$ and of the stable manifold of $x''$, for $\epsilon = 10^{-4}$. We remark that with a correction $\Delta x''$ characterized by $\Delta I_2''$ of order $10^{-8}$ the point $\phi^T(x' + \Delta x') + \Delta x''$ belongs to the stable manifold of $x''$.

$\varphi_2 = 0$), we define the "geometrical" diffusion coefficient $\mu$ as the limit of the quantity:

$$G(t) = \frac{\lambda d(s(t))}{\ln(s(t)/s(0))} \quad , \tag{27}$$

where we defined $s(t) = s(0)\exp(\lambda\ t)$. For $\epsilon = 10^{-5}$ we can infer from (figure 15,right) a value of $\mu = 7\,10^{-11}$. We have repeated the computation of $\mu$ for different values of $\epsilon$ up to $\epsilon = 10^{-3}$, i.e. close to the thresholds for diffusion on

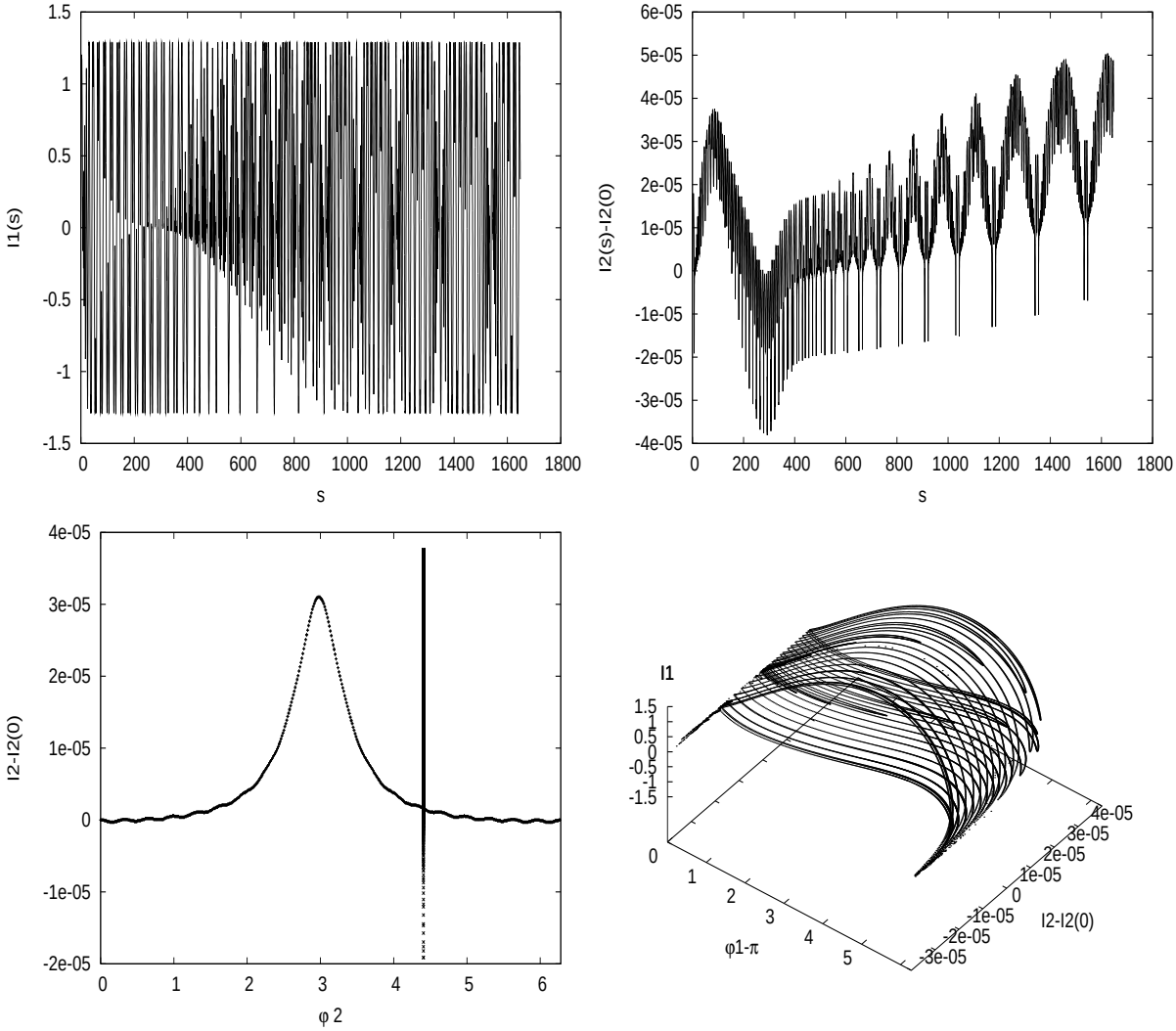


**Fig. 12.** Computation of the unstable manifold for an initial condition $(\varphi_1, \varphi_2, I_1, I_2) = (\pi, 0, 0, 0.324)$ on a KAM torus of $\phi_{|\Lambda}$ for $\epsilon = 10^{-6}$. The initial conditions for the computation of the manifold after $k = 10^5$ iterations are $x = (\pi, 4.406484, 0, 0.324001)$. **On the top:** Representation of $I_1(s)$ (on the left) and $I_2(s)$ (on the right). **On the bottom left:** The orbit of $\phi_{|\Lambda}$ is on a KAM torus. The vertical segment corresponds to the representation on the plane $(I_2 - I_2(0), \varphi_2)$ of the points of $W_u(x)$ with $|\varphi_1 - \pi| \leq 0.5$ (reducing the tolerance on $\varphi_1$ decreases the number of points on the figure, but does not decrease the amplitude of the segment). The fluctuations of $W_u(x)$ along $I_2$ are definitely bigger than the variation of $I_2$ along the torus. **On the bottom right:** Representation of the unstable manifold of $x$ in the three dimensional space $\varphi_1$, $I_2 - I_2(0)$,$I_1$.

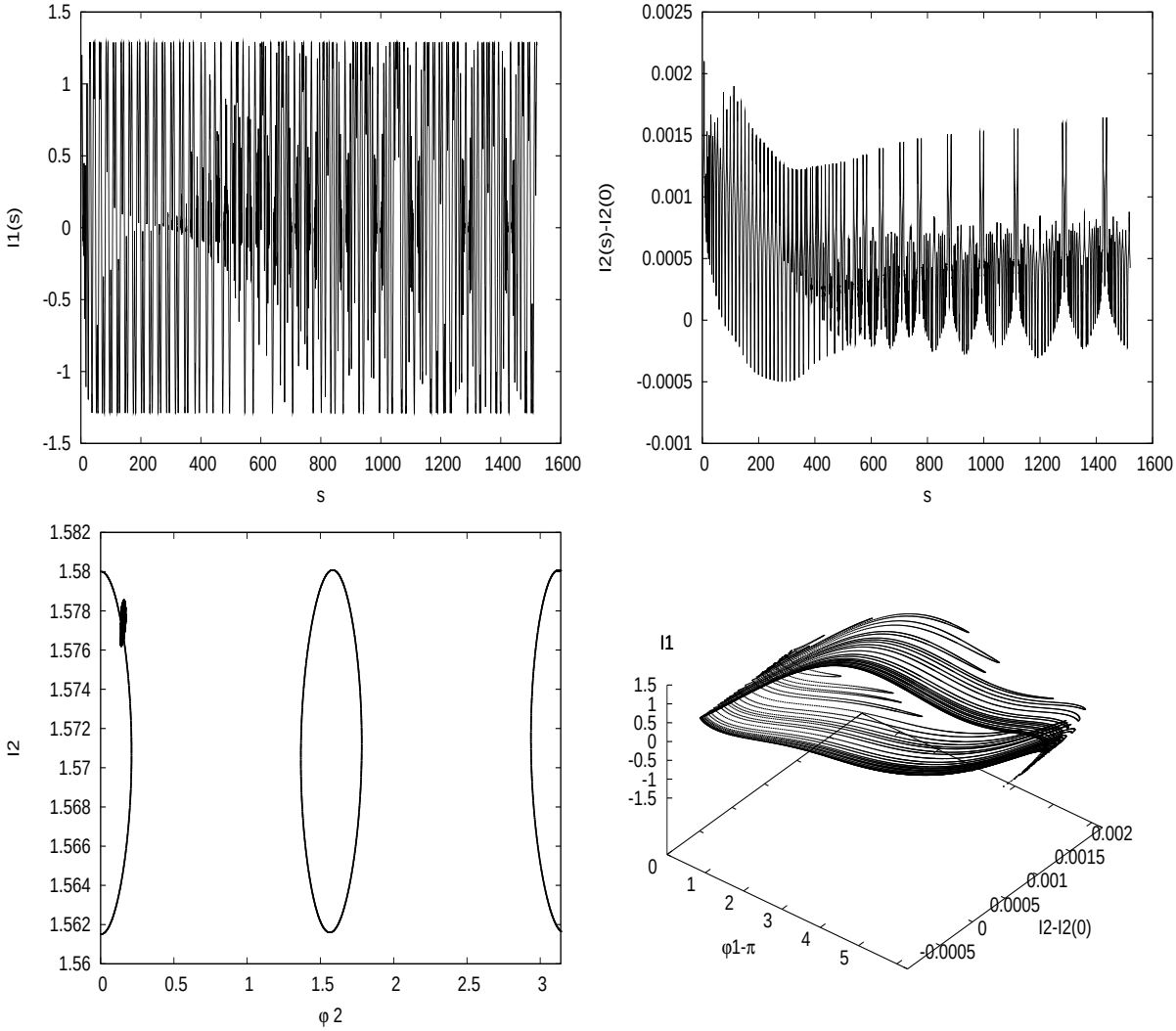


**Fig. 13.** Computation of the unstable manifold for an initial condition $(\varphi_1, \varphi_2, I_1, I_2) = (\pi, 0, 0, 1.58)$ on a regular resonant libration of $\phi_{|\Lambda}$ for $\epsilon = 10^{-4}$. The initial conditions for the computation of the manifold after $k = 10^5$ iterations are $x = (\pi, 0.153, 0, 1.576)$. **On the top:** Representation of $I_1(s)$ (on the left) and $I_2(s)$ (on the right). **On the bottom left:** The orbit of $\phi_{|\Lambda}$ is on a regular resonant libration. The small vertical segment corresponds to the representation on the plane $(I_2, \varphi_2)$ of the points of $W_u(x)$ with $|\varphi_1 - \pi| \leq 0.5$ (reducing the tolerance on $\varphi_1$ decreases the number of points on the figure, but does not decrease the amplitude of the segment). The amplitude of 2 $10^{-3}$ of this segment in the direction of $I_2$ is representative of the spread of $W_u(x)$ along this direction. **On the bottom right:** Representation of unstable manifold of $x$ in the three dimensional space $\varphi_1$, $I_2$,$I_1$.

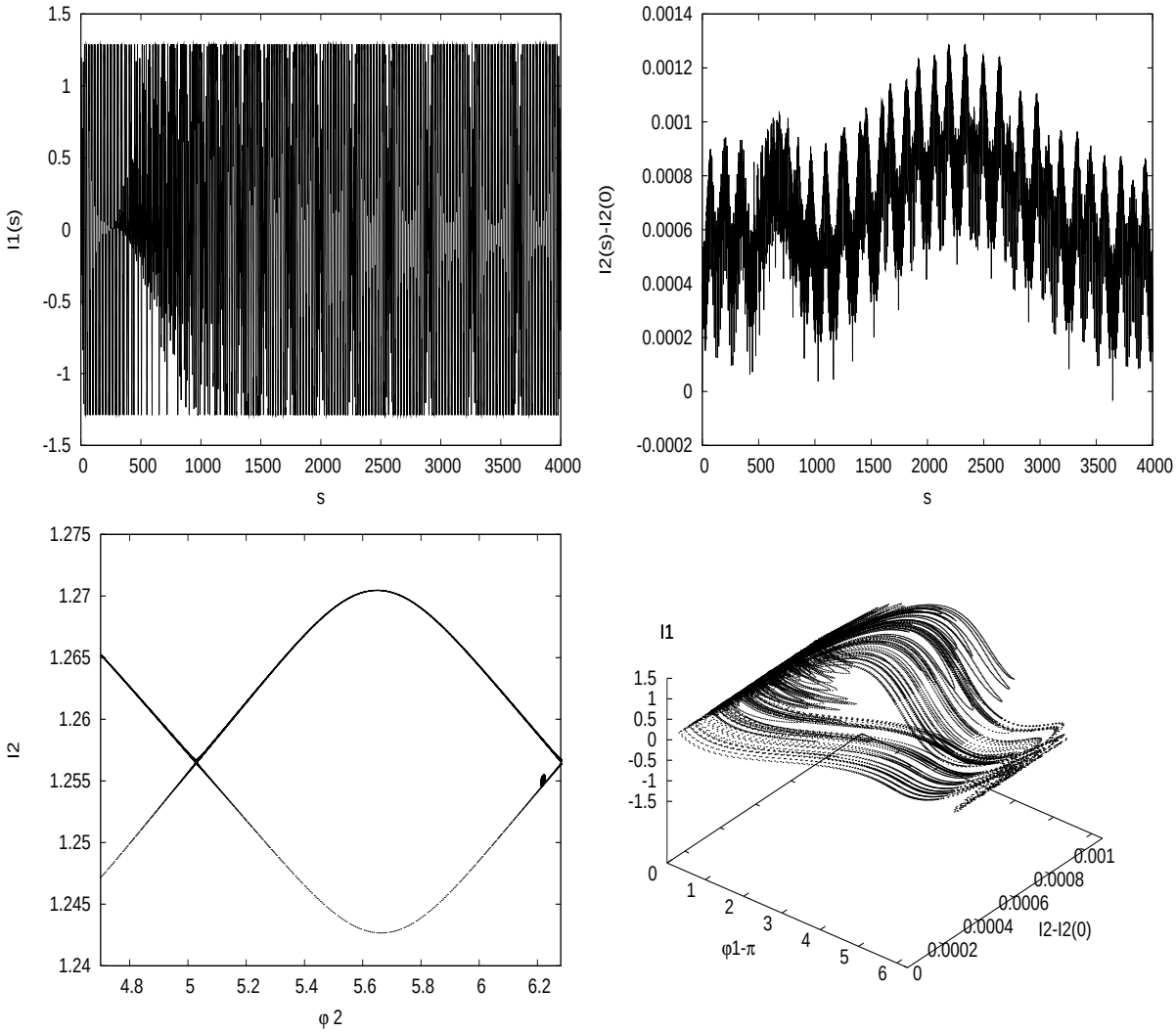


**Fig. 14.** Computation of the unstable manifold for an initial condition $(\varphi_1, \varphi_2, I_1, I_2) = (\pi, 0, 0, 1.256)$ on a chaotic resonant orbit of $\phi_{|\Lambda}$ for $\epsilon = 10^{-4}$. The initial conditions for the computation of the manifold after $k = 10^5$ iterations are $x = (\pi, 6.213, 0, 1.254)$. **On the top:** Representation of $I_1(s)$ (on the left) and $I_2(s)$ (on the right). **On the bottom left:** The orbit of $\phi_{|\Lambda}$ is chaotic. The small vertical segment corresponds to the representation on the plane $(I_2, \varphi_2)$ of the points of $W_u(x)$ with $|\varphi_1 - \pi| \leq 0.5$ (reducing the tolerance on $\varphi_1$ decreases the number of points on the figure, but does not decrease the amplitude of the segment). The amplitude of 1.5 $10^{-3}$ of this segment in the direction of $I_2$ is representative of the spread of $W_u(x)$ along this direction. **On the bottom right:** Representation of unstable manifold of $x$ in the three dimensional space $\varphi_1$, $I_2$,$I_1$.

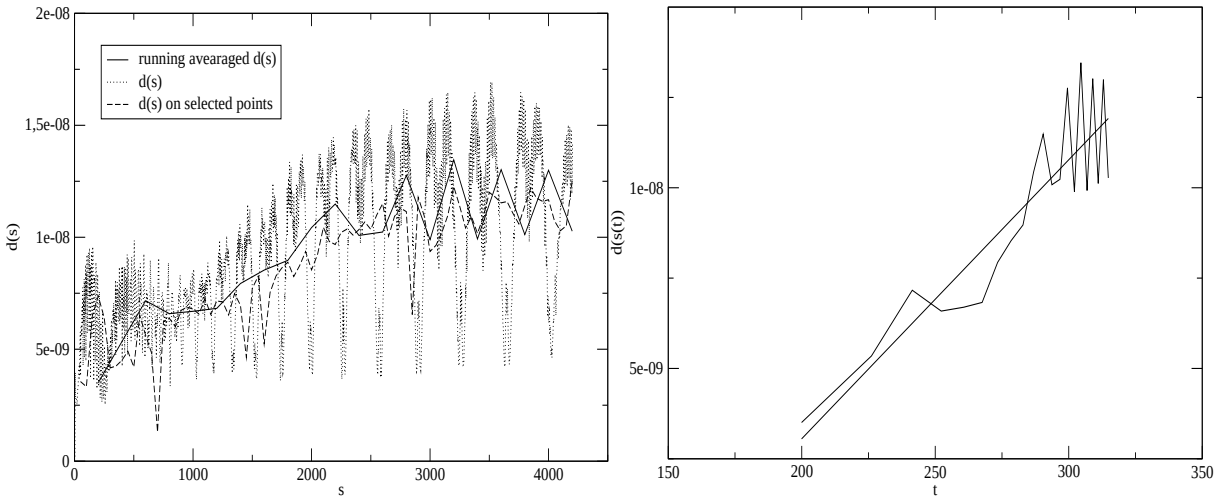


**Fig. 15. On the left:** plot of $d(s)$ versus $s$ for $\epsilon = 10^{-5}$ ($N = 200$, the initial conditions are $I_1 = 0$, $\varphi_1 = \pi$, $0.6 < I_2 < 1$, $\varphi_2 = 0$). The running average over a length $\Delta s = 200$ as well as the quantity $d(s)$ computed selecting the data with $|\varphi_1 - \pi| \leq 0.5$ are also plotted. **On the right:** plot of the quantity $d(s(t))$ defined in the text for the averaged data of left panel and its linear interpolation.

$\Lambda$ but still below this thresholds. We report in figure 15 the comparison with the diffusion coefficient computed as reported in figure 2. With respect to figure 2 we have added the diffusion coefficient computed on a set of $N = 100$ initial conditions near $I_2 = 0.8$, i.e. in the same domain used for computing $d(s)$. The geometrical diffusion coefficient shows a remarkable agreement with the spread of orbits in the $I_2$ direction quantified by $D$. Although we are aware that this result is based on the detection of finite pieces of the unstable manifolds, the agreement with the diffusion coefficient on individual orbits confirms that the spread of the manifolds is significant to explain the diffusion that we detected numerically in section 2.

## 7. Statistical analysis of Arnold diffusion

In this section we describe the methods that we use to estimate the diffusion coefficients for the diffusion of orbits with initial conditions in a neighbourhood of the hyperbolic invariant manifold for the map (10). We remark that the map (10) depends periodically on all the actions. This property simplifies the definition of the diffusion process because, in principle, the actions are allowed to diffuse indefinitely on $\mathbb{R}^2$.

Method (m1) is purely a phenomenological one: the diffusion coefficient related to the action $I_2$ of a set of $N$ orbits is measured as the average slope

$$\frac{\sum_{j=1}^{N} |I_2^{(j)}(t) - I_2^{(j)}(0)|^2}{N} \quad . \tag{28}$$

For the justification of this method we refer to figure 1, which shows that the evolution with time of the mean square distance of a set of $N = 1000$ orbits

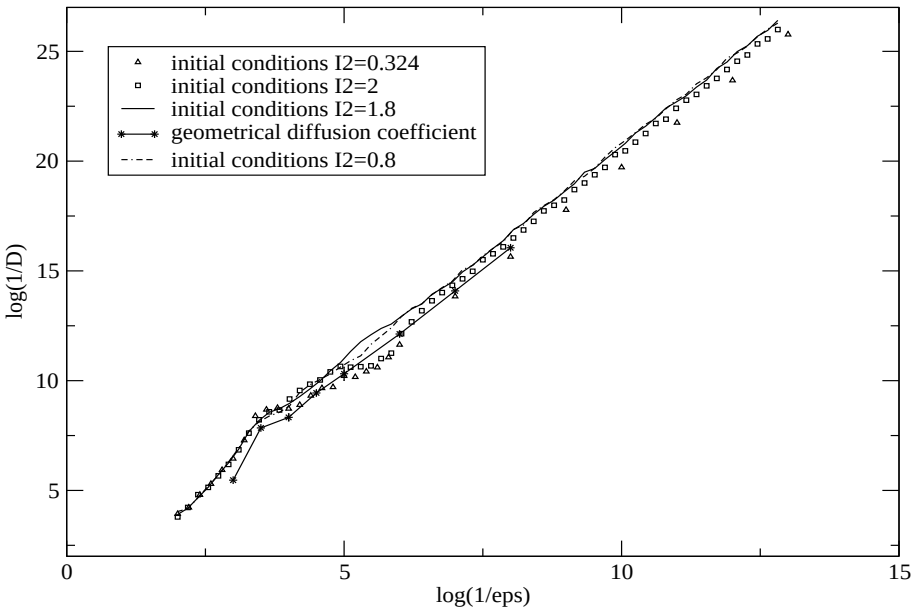


**Fig. 16.** Variation of the diffusion coefficient as a function of $\epsilon$ for four sets of $N = 100$ initial conditions. The geometrical diffusion coefficient $\mu$ defined in the test shows a remarkable agreement with the spread of particles in the $I_2$ direction quantified by $D$.

from their initial conditions could be well fitted by a linear law, whose slope is identified as the diffusion coefficient of the sets of orbits. This method is purely phenomenological because no prescriptions are given about the choice of the $N$ initial conditions, of the time interval used to fit the diffusion coefficient, and it is not based on any statistical model for the diffusion process. However, it is very useful as a first test which provides hints about the existence of some kind of statistical diffusion related to the variations of the action $I_2$. One of the technical drawbacks which one encounters in the application of this method is related to the fact that, for small values of the perturbing parameter, the average growth of (28) can be masked by larger short period oscillations for very long times. This problem specifically affects the measures of diffusion coefficients for quasi–integrable systems at small values of the perturbing parameter, and it was solved in [23] with a modification of method (m1), which we denote by (m2). Method (m2), which was used to compute the values of figure 2, is based on the following consideration: the oscillations in the evolution of (28) which are correlated to the variations of the angles $\varphi_1, \varphi_2$ can be reduced by taking into account in the average (28) only the points $(\varphi_1(t), \varphi_2(t), I_1(t), I_2(t))$ of the orbits such that $\varphi_1(t), \varphi_2(t)$ are returned near the initial values $\varphi_1(0), \varphi_2(0)$. Because not for all the $N$ points the angles return near their initial value at the same time $t$, we fix two parameters $\Delta T, c$ and we denote $t_i = i\Delta T$ and by $N(i)$ the number of points such that:

$$|\varphi_1(t) - \varphi_1(0)| + |\varphi_2(t) - \varphi_2(0)| \leq c$$

for some $t \in [t_{i-1}, t_i]$. We also denote by $A(i)$ the set of all these points, by:

$$d(t_i) = \sum_{x=(\varphi_1(t),\varphi_2(t),I_1(t),I_2(t))\in A(i)} \frac{|I_2(t) - I_2(0)|^2}{N(i)} \quad , \tag{29}$$

and by $\sigma(t_i)$ the standard deviation of $|I_2(t) - I_2(0)|^2$ in the interval $[t_{i-1}, t_i]$.

Then, we fit the finite sequence $d(t_1), \ldots, d(t_K)$ to a linear law by means of a chi–square method, and the slope of the linear law will be identified as the diffusion coefficient. The chi–square method provides also an error on the slope based on the individual values of $\sigma(t_1), \ldots, \sigma(t_K)$. The values of the parameters $c, \Delta T$ must be balanced so that to have points in the set $A(i)$, and specific choices will determine different errors. The value of the parameter $K$ must be chosen so large that the chi–square fit is good, which means that the average growth of the $d(t_i)$ dominates the residual short period oscillations.

The third method (m3) is based on a statistical model for the diffusion of the action $I_2$. We consider a curve $\gamma \subseteq \Lambda$ defined by:

$$\gamma = \{(\varphi_1, \varphi_2, I_1, I_2) \ \text{ with } \ \varphi_1 = \pi, \varphi_2 = 0, I_1 = 0\} \quad ,$$

which is parametrized by the action $I_2$. Then, we choose a neighbourhood $W$ of $\gamma$ and perform a statistical analysis on the variations of $I_2$ for orbits with initial conditions in $W$. For initial conditions $x = (\varphi_1, \varphi_2, I_1, I_2) \in W \backslash \Lambda$ we define the return map to $W$ as follows: if there exists a minimum integer $t(x) \geq 1$ such that $\phi_\epsilon^{t(x)-1}(x) \notin W$ and $\phi_\epsilon^{t(x)}(x) \in W$, we denote $\psi(x) = \phi_\epsilon^{t(x)}(x)$. The set $W_*$ on which $\psi$ is defined can be a proper subset of $W$, but for the Poincaré recurrence theorem (which applies to the present case because the map $\phi_\epsilon$ is periodic with respect to the actions) it has the same Lebesgue measure as $W$.

Then, let us denote $\pi(x) = I_2$, and by $X_i(x) = \pi(\psi^{i+1}(x)) - \pi(\psi^i(x))$. A statistical approach to the dynamics in $W_*$, such as the one described in [32], would be justified by the existence of a set $\tilde{W}_* \subseteq W_*$ of points $x$ such that the sequence $X_1, X_2, ...$ is a sequence of independent random variables. This is a very strong requirement that, in our knowledge, can represent only an approximate description of the dynamics of the system. In this spirit, the traditional statistical approaches, such as for example those based on random phases approximations, replace first the true dynamics with an approximate one which behaves as a Markovian process, and then compute statistical quantities that can be defined precisely via the Markovian approximation.

Here, we proceed in a different way: we fix a set $W$ and then, instead of performing statistical approximations on the dynamics, we check that finite sets of initial conditions and the finite sequence $X_1, ...., X_T$ averaged over these initial conditions behave as if the process would be approximately Markovian. Because the variables $X_1, ...., X_T$ have the same mean and variance, but are not necessarily normally distributed, we check that the variable $Y_T = \frac{X_1 + ... + X_T}{T}$ is normally distributed within a tolerance admitted for the central limit theorem convergence. Precisely, we require that the average of $Y_T$ over a set of $N$ initial conditions $x_1, \ldots, x_N$ are such that:

s1) denoting by $E(Y_T) = \frac{1}{N}\sum_{j=1}^{N} Y_T(x_j)$ the average of the variable $Y_T$ over the set of $N$ initial conditions $x_1, \ldots, x_N$, we require:

$$|E(Y_T)| \leq \frac{1}{\sqrt{N}} \sqrt{E(Y_T^2)} \quad ; \tag{30}$$

s2) the cumulative density function $\Phi_T$ of $Y_T \frac{\sqrt{T}}{\sigma}$ satisfies the Berry–Essèen inequality (see, form example, [27]):

$$\|\Phi_T(X) - \Phi(X)\| \leq C \frac{\rho}{\sigma^3 \sqrt{T}} \quad , \quad \forall X \in \mathbb{R} \quad , \tag{31}$$

with $C = 0.8$, where:

$$\sigma^2 = \frac{1}{N} \sum_{j=1}^{N} \frac{1}{T} \sum_{i=1}^{T} X_i(x_j)^2$$

is the mean variance of $X_1, ..., X_T$ averaged over the $N$ initial conditions,

$$\rho = \frac{1}{N} \sum_{j=1}^{N} \frac{1}{T} \sum_{i=1}^{T} |X_i(x_j)|^3 \quad ,$$

and $\Phi(x)$ is the cumulative normal distribution defined by:

$$\Phi(X) = \frac{1}{2} \Big( 1 + \mathrm{erf} \Big( \frac{X}{\sqrt{2}} \Big) \Big) \quad . \tag{32}$$

By denoting:

$$T_0 = \min_{i=1,...,N} \Big( \sup_{j=1,...,T} t(\psi^j(x_i)) \Big) \quad , \tag{33}$$

we say that a set of $N$ initial conditions has regular statistics on the time $T_0$ if it satisfies conditions (s1),(s2) with respect to the parameter $T$ appearing in (33).

Then, we compute the diffusion coefficient $D$ on the set of $N$ initial conditions $x_1, \ldots, x_N$ as if the process would be a Markovian one, as the following average:

$$D = \frac{1}{N} \sum_{j=1}^{N} \frac{1}{T} \sum_{i=1}^{T} \frac{X_i(x_j)^2}{t_i(x_j)}$$

where $t_i(x_j) = t(\psi^{i-1}(x_j))$ denotes the i–th return time of the j–th particle.

**Remarks.** (i) The quantity $D$ is different from the variance $\sigma^2$ because it takes into account the individual return times $t_i(x_j)$.
(ii) In view of the central limit theorem, the diffusion coefficient and the variance of the variable $Y_T$ are computed by averaging over the variables $X_i$, while their errors are estimated as the normal errors of the normal distribution of $Y$. Therefore, the error on $D$ can be estimated by $D\sqrt{2/N}$.
(iii) The results of this statistical analysis depend on the choice of $W$: on the one hand, we expect that the dynamics in neighbourhoods of $\gamma$ better approximates a Markovian process by restricting the neighbourhood $W$; on the other hand, for $\epsilon = 0$ it is $X_i(x) = 0$ for all $i$ and for all $x \in W$, for any choice of the neighbourhood $W$.

In figure 17 we compare the computation of the diffusion coefficients computed with the methods (m2) and (m3) for the same set of initial conditions used to produce figure 2, and we reported only the results of integrations satisfying

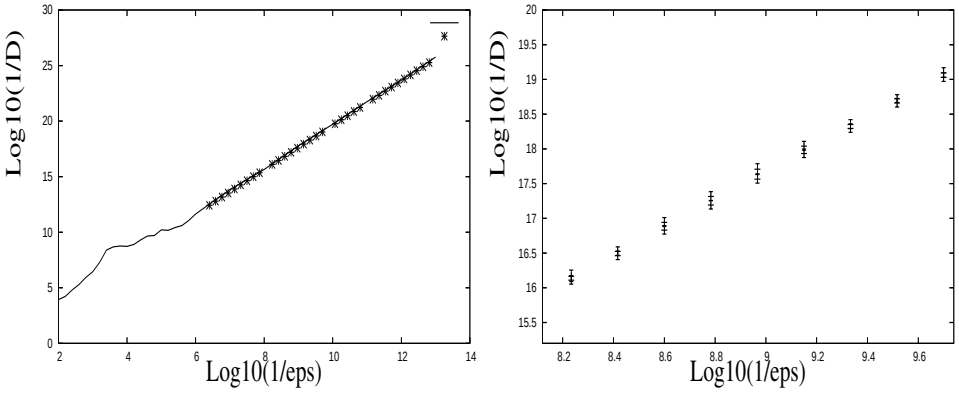


**Fig. 17.** Comparison of the diffusion coefficients computed with methods (m2) and (m3) for the set of initial conditions used to produce figure 2 with $I_2 = 0.324$. **On the left:** The continuous line represents the results obtained with method (m2); the stars correspond to the results obtained with method (m3), but only the data satisfying (s1), (s2) are represented. We remark that only the data in the regime of validity of the Melnikov approximation turn out to satisfy (s1), (s2). **On the right:** Representation of a zoom of the data of the left panel with their error bands. Because the details of the two methods are different, in particular the total integration time, the two bands do not always agree, although the differences are not remarkable.

conditions (s1), (s2). For the (m3) method we used 100 return times to a set $W$ defined by:

$$W = \{(I_1, \varphi_1, I_2, \varphi_2) : \max\{|I_1|, |\varphi_1 - \pi|, |\varphi_2|\} < 0.01\} \quad .$$

It is remarkable that only for the data in the regime of validity of the Melnikov approximation we observe, for all the initial conditions, 100 returns to the set $W$ satisfying the (s1), (s2) conditions.

## 8. Conclusions

In this paper we have studied the Arnold diffusion along a normally hyperbolic manifold $\Lambda$ for a model of a priori unstable dynamical system. We have numerically detected the stable and unstable manifolds of $\Lambda$. We have introduced a definition of Arnold diffusion which can be numerically investigated, and we have shown that the numerically computed stable and unstable manifolds indeed support this kind of Arnold diffusion. We also have shown that the global topology of the stable and unstable manifolds has a topological transition when the Melnikov approximation is not valid. This transition is correlated to a change of the law of dependence of the diffusion coefficient on the perturbing parameter. This suggests that the Melnikov approximation is not only a technical tool which allows one to compute accurate approximations of the manifolds at small values of the perturbing parameters, but is related to a dynamical regime, and it would be favorable to use it to explain the statistical properties of Arnold diffusion.

**Acknowledgments.** M. Guzzo has been supported by the project CPDA063945/06 of the University of Padova.

## References

1. Arnold V.I.: Instability of dynamical systems with several degrees of freedom. Sov. Math. Dokl., 6, 581–585, 1964.
2. Berti M., Biasco L. and Bolle P.: Drift in phase space: a new variational mechanism with optimal diffusion time. J. Math. Pures Appl., Vol. 9, 82, no. 6, 613–664, 2003.
3. Berti M. and Bolle P.: A functional analysis approach to Arnold diffusion. Annales de lInstitut Henri Poincare (C) Non Linear Analysis, Vol. 19, 4, 395-450, 2002.
4. Bessi U., Chierchia L. and Valdinoci E.: Upper bounds on Arnold diffusion times via Mather theory. J. Math. Pures Appl., Vol. 80, 105–129, 2001.
5. Broer H.W., Osinga H.M. and Vegter G.: Algorithms for computing normally hyperbolic invariant manifolds. ZAMP, 48, 480-524, 1997.
6. Chierchia L. and Gallavotti G.: Drift and diffusion in phase space. Ann. Inst. H.Poincaré, Vol. 60, 1–144, 1994.
7. Chirikov B.V.: Research concerning the theory of nonlinear resonance and stochasticity", Preprint N 267, Institute of Nuclear Physics, Novosibirsk (1969) Engl. Trans., CERN Trans. 71-40 (1971).
8. Delshams A., de la Llave R. and Seara T.M.: A geometric mechanism for diffusion in Hamiltonian systems overcoming the large gap problem: heuristics and rigorous verification on a model. Mem. Amer. Math. Soc. 179, no. 844, 2006.
9. Efthymiopoulos, C.; Contopoulos, G.; Voglis, N.: Cantori, Islands and Asymptotic Curves in the Stickiness Region. Celestial Mechanics and Dynamical Astronomy, v. 73, Issue 1/4, 221-230, 1999.
10. Froeschlé C., Lega E. and Gonczi R.: Fast Lyapunov indicators. Application to asteroidal motion. Celest. Mech. and Dynam. Astron., Vol. 67, 41–62, 1997.
11. Froeschlé C., Guzzo M. and Lega E.: "Graphical Evolution of the Arnold Web: From Order to Chaos". Science, Volume 289, n. 5487, 2000.
12. Froeschlé C., Lega E.: On the Structure of Symplectic Mappings. The Fast Lyapunov Indicator: a Very Sensitive Tool, Celestial Mechanics and Dynamical Astronomy, 78, Issue 1/4, p. 167-195, 2000.
13. Froeschlé C., Guzzo M. and Lega E.: "Local and global diffusion along resonant lines in discrete quasi–integrable dynamical systems", Celestial Mechanics and Dynamical Astronomy, vol. 92, n. 1-3, 243-255, 2005.
14. Guzzo M., Lega E. and Froeschlé C.: On the numerical detection of the effective stability of chaotic motions in quasi-integrable systems. Physica D, Volume 163, Issues 1-2, 1-25, 2002.
15. Guzzo M., Lega E. and Froeschlé C.: "First Numerical Evidence of Arnold diffusion in quasi–integrable systems". DCDS B, vol. 5, n. 3, 2005.
16. Guzzo M., Lega E. and Froeschlé C.: Diffusion and stability in perturbed non-convex integrable systems. Nonlinearity, 19, pp 1049–1067, (2006).
17. Hénon M. and Heiles C.: The Applicability of the Third Integral of Motion: Some Numerical Experiments. The Astronomical Journal, 69, p. 73–79, (1964).
18. Hasselblatt B. and Pesin Y.: Partially hyperbolic dynamical systems. Handbook of dynamical systems. Vol. 1B, 1–55, Elsevier B. V., Amsterdam, 2006.
19. Hirsch M.W., Pugh C.C. and Shub M.: Invariant Manifolds. Lecture Notes in Mathematics, Vol. 583. Springer-Verlag, Berlin-New York, 1977.
20. Krauskopf, B., Osinga, H.M., Doedel, E.J., Henderson, enheimer, J., Vladimirsky, A., Dellnitz, M., Junge, O.: A survey of methods for computing (un)stable manifolds of vector fields. Int. J. Bif. and Chaos, 15, 763-791, 2005.
21. Konishi T. and Kaneko K.: Diffusion in Hamiltonian chaos and its size dependence. J. Phys. A: Math. Gen., 23, 15, L715-L720.
22. Laskar J.: Frequency analysis for multi-dimensional systems. Global dynamics and diffusion. Physica D, 67, pp 257–281, (1993).
23. Lega E., Guzzo M. and Froeschlé C.: "Detection of Arnold diffusion in Hamiltonian systems". Physica D, vol. 182, p. 179–187, 2003.
24. Lega E., Froeschlé C. and Guzzo M.: "Diffusion in Hamiltonian quasi–integrable systems." In Lecture Notes in Physics 729, "Topics in gravitational dynamics", Benest, Froeschlé, Lega eds., Spinger, 2007.

25. Lichtemberg A. and Aswani M.A.: Arnold diffusion in many weakly coupled mappings. Phys. Rev. E, 57, 5, 5325–5321, 1998.
26. MacKay R.S., Meiss J.D. and Percival I.C.: Transport in Hamiltonian Systems. Physica D, 13, 55–81, 1984.
27. Manoukian, E.: Modern Concepts and Theorems of Mathematical Statistics. Springer, 1986.
28. Simo C.: On the analytical and numerical approximation of invariant manifolds, in Modern Methods in Celestial Mechanics, D. Benest, Cl. Froeschlé eds, Editions Frontières, 285-329, 1989.
29. Simo C. and Valls C.: A formal approximation of the splitting of separatrices in the classical Arnold's example of diffusion with two equal parameters. Nonlinearity 14, no. 6, 1707–1760, 2001.
30. Treschev D.: Trajectories in a neighbourhood of asymptotic surfaces of a priori unstable Hamiltonian systems. Nonlinearity 15 2033-2052, 2002.
31. Treschev D.: Evolution of slow variables in a priori unstable Hamiltonian systems. Nonlinearity 17 1803-1841, 2004.
32. Varvoglis H.: "Chaos, random walks and diffusion in Hamiltonian systems." In Hamiltonian systems and Fourier Analysis, 247–287. Benest, Froeschlé and Lega editors. Cambridge Scientific Publishers, 2005.
33. Wood B.P., Lichtenberg A. and Lieberman M.A.: Arnold diffusion in weakly coupled standard map. Phys. Rev. A, 42, 5885-5893, (1990).

Communicated by